The Dissertation Committee for Talha Ijaz Certifies that this is the approved version of the following dissertation:

Fibroblasts: Key Cells in Inflammation and Fibrosis

Committee:

Allan R. Brasier, M.D., Supervisor and Mentor

Ronald G. Tilton, Ph.D., Co-Mentor

N. Muge Kuyumcu-Martinez, Ph.D., Chair

Iryna V. Pinchuk, Ph.D.

Kenichi Fujise, M.D.

Dianna M. Milewicz, M.D., Ph.D.

Dean, Graduate School

Fibroblasts: Key Cells in Inflammation and Fibrosis

by

Talha Ijaz, B.Sc.

Dissertation

Presented to the Faculty of the Graduate School of

The University of Texas Medical Branch

in Partial Fulfillment

of the Requirements

for the Degree of

Doctor of Philosophy

The University of Texas Medical Branch

May, 2018

Dedication

This is dedicated to my father, Hafiz Ijaz Ahmad, and my mother, Fauzia Naheed, who set an impeccable example for me as devoted physicians and community leaders and nurtured in me the desire to pursue scientific discovery; to my sisters Khadija, Amna, Maria and Ramla, who kept me engaged in their lives from afar; to my dear wife Umaymah Shahid, who provided me with unwavering support through the highs and lows of my research; and to my mentors Dr. Allan R. Brasier and Dr. Ronald G. Tilton, who accepted me into their lab and gave me an extraordinary opportunity to uncover basic biological truths. In addition, this is dedicated to the numerous other family members, friends and co-workers who helped me along the way and made this journey possible.

Acknowledgements

I would like to thank my co-mentors, Dr. Allan R. Brasier and Dr. Ronald G. Tilton, for their continuous support and encouragement during my graduate training. In addition, I would like to appreciate the guidance provided to me by my dissertation committee members including Dr. Muge Martinez, Dr. Iryna Pinchuk, Dr. Ken Fujise and Dr. Dianna Milewicz. I am grateful to Dr. Adrian Recinos III for helping me get started with lab work, to Hong Sun for the continuous help with my animal experiments, to Dr. Bing Tian for sharing his scientific insights, to Dr. Mohammad Jamaluddin for his collaboration with the hypertrophic scar fibroblast studies and to Dr. Jun Yang for helping me troubleshoot my experimental assays. Lastly, a special thanks to Mark Griffin in the UTMB Flow Cytometry Core in assisting me with my flow cytometry experiments.

The work presented here was partly supported by Ruth L. Kirschstein Pre-doctoral National Research Service Award from NHLBI (F30HL128036) to Talha Ijaz.

Fibroblasts: Key Cells in Inflammation and Fibrosis

Publication No._____

Talha Ijaz, Ph.D.

The University of Texas Medical Branch, 2018

Supervisor: Allan R. Brasier

Abstract: Angiotensin II (Ang II) infusion into normolipidimic mice leads to the development of aortic dissections and abdominal aortic aneurysm (AAA). IL-6 is a pro-inflammatory cytokine that is secreted by fibroblasts and macrophages in the aortic adventitia and promotes the development of aortic dissections. In our previous work, analysis of aortic adventitial fibroblast secretions *in vitro* suggested that aortic fibroblasts were the main producers IL-6. Furthermore, our lab has demonstrated that Ang II activates the transcription factor nuclear factor- kappa B/ RelA, which binds to the IL-6 promoter and promotes transcription. To investigate the role of fibroblast-RelA in Ang II mediated AAA formation, I aimed to generate fibroblast-specific RelA-deficient mice using Cre-Lox technology. Mice containing Cre recombinase under the transcriptional control of collagen 1α2 promoter fused with a modified estrogen receptor, which could be temporally activated with tamoxifen (Col1a2-CreER^T), undergo targeted genetic recombination in aortic fibroblasts. Using mT/mG Cre-reporter mice harboring Col1a2-CreER^T, I provide evidence that Col1a2-CreER^T is activated by tamoxifen in both adventitial fibroblasts and in vascular smooth muscle cells (VSMCs). Interestingly, I observed that deletion of RelA from aortic VSMCs and fibroblasts, using Col1a2-CreER^T mice containing RelA-flox alleles, protects from Ang II mediated AAA formation. Furthermore, aortic-RelA deficient

animals have decrease production of pro-inflammatory cytokines IL-6 and IL-1β, and decrease recruitment of CD11b+F4/80^{lo}Ly6C^{hi} inflammatory monocytes into the aortic wall during Ang II infusion. Ang II is also a potent inducer of TGFβ, a cytokine that promotes fibroblast to myofibroblast transdifferentiation. We hypothesized that TGFβ induces myofibroblast transdifferentiation via activation of fibroblast-RelA, an event that may precede the development of vascular inflammation and AAA formation. Using primary human fibroblasts, I demonstrate that TGFβ is a potent inducer of Smad2/3 signaling but not of RelA signaling in fibroblasts. Furthermore, RelA is dispensable for myofibroblast transformation. In contrast, Smad3 promotes the transcription of myofibroblast genes including Nox4, SM22α, collagen 1α1 and fibronectin. Investigation of transcriptional co-activators that promote phosphorylation of RNA polymerase II for transcription elongation of target genes suggests that both BRD4 (bromodomain and ET domain containing protein 4) and CDK9 (cyclin dependent kinase 9) are needed for myofibroblast transformation. I further identify a small molecule inhibitor of BRD4, JQ1, which can not only prevent but also reverse the myofibroblast phenotype in cells taken from hypertrophic scars of burn patients. In conclusion, my work suggests that fibroblast-RelA is not necessary for myofibroblast transdifferentiation but it plays pivotal role in Ang II mediated vascular inflammation and AAA formation.

TABLE OF CONTENTS

List of Tables

List of Figures

List of Abbreviations

Ang II- Angiotensin II
AAA- Abdominal aortic aneurysm
αSMA- smooth muscle alpha actin
Col1- Collagen 1
Col1a2-CreER^{T} – Col1α2-promoter driven Cre recombinase fused with modified estrogen receptor
NF-κB- Nuclear factor- kappa B
Nox4- NADPH oxidase 4
RelA f/f- RelA flox alleles
SM22α- Smooth muscle protein 22 alpha
TGFβ- Tumor growth factor beta
WT- Wild-type
QRT-PCR- Quantitative reverse transcriptase- polymerase chain reaction

Chapter 1: Role of Fibroblast in Inflammation, Wound Healing and Fibrosis

Fibroblasts are spindle-shaped cells found in the stroma of most tissues and have varying roles during development, wound healing and in disease. Fibroblasts are considered to be a diverse population of cells with different gene expression programs depending on the site of origin and therefore they do not have a specific set of differentiating markers (1). In skin, fibroblasts populate the dermis and secrete extracellular matrix (ECM) proteins such as collagen that provide the skin with tensile strength. Similarly, aortic fibroblasts are mostly found outside of the blood vessel in the adventitia surrounded by ECM and help to maintain vascular integrity. The work presented here examines two different populations of fibroblasts, dermal and aortic, in deciphering the role of nuclear factor- kappa B (NF-κB)/RelA transcription factor in inflammation and in myofibroblast transdifferentiation. Although the original intent was to investigate the mechanism of aortic fibroblast to myofibroblast transdifferentiation, primary human adventitial fibroblasts underwent senescence within 5-6 passages in cell culture and therefore were not a feasible model to study. In contrast, primary human dermal fibroblasts continuously proliferated and maintained their original morphology even after 14 passages making them an ideal cell model for my investigation of myofibroblast transdifferentiation. In addition, an *in vivo* mouse model was utilized to determine the role of aortic fibroblast in mediating vascular inflammation.

ANGIOTENSIN II INDUCES VASCULAR INFLAMMATORY DISEASES

Angiotensin II (Ang II) is a small octapeptide that is well known to be involved in regulation of blood pressure and sodium homeostasis (2). Angiotensinogen is the precursor protein that is cleaved by the enzyme renin to Ang I, which is further processed by

angiotensin converting enzyme (ACE) to Ang II. In addition to regulation of blood pressure, it is now well appreciated that Ang II is a potent mediator of vascular inflammation. For example, hypercholesterolemia increased circulating angiotensin peptides (Ang II, III, IV, and 4-8) and induced development of atherosclerosis, a vascular inflammatory disease, which was significantly blunted in Ang II receptor type 1a (AT1a)-deficient mice (3). Furthermore, continuous infusion of Ang II via mini-osmotic pumps into hyperlipidemic mice augmented atherosclerosis and induced more secretion of inflammatory cytokines from the vessel wall (4, 5). In 2001, Daugherty et al., demonstrated that infusion of Ang II into hyperlipidemic mice also led to the development of abdominal aortic aneurysm (AAA) that localized to the supra-renal region of the aorta (6). Ang II induced AAAs are preceded by aortic dissections and have massive accumulation of monocytes localized to the region of aneurysm formation (7, 8). The renin-angiotensin system also contributes to human atherosclerosis. In a randomized, multi-center clinical trial OLIVUS, administration of angiotensin receptor blocker (ARB) Olmesartan decreased progression of coronary atherosclerosis as assessed by intravascular ultrasound (9). More recently, a cross-sectional retrospective study analyzing effect of ACE inhibitors or ARBs on mortality from AAA rupture revealed a significant protective effect in patients who received the targeted drugs versus those who received a placebo (10). Collectively, these lines of evidence suggest a pathological role of an overactive renin-angiotensin system, and specifically of Ang II in mediating vascular inflammatory diseases.

INFLAMMATION IS A REGULATED PROCESS

Infection or injury to a tissue triggers an inflammatory response that has been classically characterized by redness, pain, swelling and some organ dysfunction (11). At the cellular level, a non-specific injury to a vessel wall leads to influx of circulating leukocytes, specifically monocytes, and T cells (12). This is a coordinated process with injured tissue increasing expression of cell adhesion molecules, chemokines and cytokines

that direct the circulating leukocyte extravasation across the endothelium into the tissue. Local cytokines activate monocytes/macrophages and promote the clearance of cellular debris (11). Resolution of the inflammation is key to attaining homeostasis whereas prolonged inflammation or dysregulation of this process is linked to the development of multiple disease states including type 2 diabetes, atherosclerosis and AAA (11, 12).

ANG II ACTIVATES NUCLEAR FACTOR-KAPPA B, A MASTER REGULATOR OF INFLAMMATION

Cytokines, growth factors and pathogen associated molecular patterns (PAMPs) bind to cell surface receptors triggering signaling cascades that lead to the activation of the NF-kB transcription factors. NF-kB is well known to stimulate two initial key steps, leukocyte adherence and chemotaxis, that promote the development of vascular inflammation (12). Leukocyte adherence occurs by increase expression of cell surface adhesion molecules including vascular cell adhesion molecule-1 (VCAM-1), intercellular adhesion molecule-1 (ICAM-1) and E-selectin, all proteins that are transcriptionally regulated by NF-kB. In addition, chemotaxis is promoted by NF-kB dependent chemokines such as monocyte chemoattractant protein- 1 (MCP-1) and granulocyte-macrophage colony-stimulating factor (GM-CSF). After monocyte recruitment, NF-kB may also be involved in macrophage activation, triggering release of anti-microbial peptides and more cytokines leading to amplification of the inflammatory response (11). Due to the multitudes of immune response genes controlled by NF-kB, it is considered a master regulator of inflammation.

NF-κB is an inducible transcription factor complex involved in the regulation of genes necessary for cell survival, differentiation, immunity and inflammation (11). RelA, C-Rel and RelB are transcription activating subunits that contain a N-terminal Rel homology domain (RHD) and a C-terminal transcription activation domain (TAD) whereas NF-κB1 (p50/p105) and NF-κB2 (p52/p100) are DNA-binding proteins that contain C-

terminal autoinhibitory ankyrin repeat domains (13). In most cells, NF-κB is high molecular weight heterodimeric complexes containing a DNA-binding- and a transcription activator subunit retained in the cytoplasm by Inhibitor of kappa B (IκB) proteins. Generally, receptor activation by a ligand triggers two signaling modules, one that induces NF-kB translocation to the nucleus and a second that regulates its activation (12). Furthermore, the kinases involved in these modules vary depending on the ligand and cell-type involved. The canonical NF-kB signaling pathway is triggered by cytokines TNFα, IL-1β and Ang II. TNFα induces the assembly of IκB Kinase (IKK) signalosome consisting of IKKα, -β and -γ. The catalytic subunit IKKβ phosphorylates IkBα on Serine residues -32 and -36 targeting it for proteolytic degradation and allowing nuclear translocation of RelA•NF-κB1 dimers, the most abundant and most potent transcription factor pair required for activation of inflammatory gene expression programs (12). In addition, an activation module is required for target gene expression. Our lab and others have demonstrated a role of reactive oxygen species (ROS) triggered activation of the catalytic subunit of protein kinase A (PKAc) leading to phosphorylation of RelA serine residue 276 (Ser276) (14). The phosphorylation of Ser276 allows for p300/CBP co-activator to bind and acetylate RelA, a necessary step for stable interaction with target DNA and gene expression.

Ang II binding to the AT1a receptor also triggers the canonical NF-κB pathway although there are some differences. In a seminal study by Cui et al., stimulation of vascular smooth muscle cells (VSMCs) with Ang II led to rapid phosphorylation of RelA Ser536 on the C-terminal TAD and increased mRNA abundance of the cytokine IL-6 (15). Ang II did not have a substantial effect on RelA Ser276 phosphorylation. Blockade of RhoA GTPase with dominant-negative RhoA expression or with exoenzyme C3 from *Clostoridium botulinium* blocked Ang II induced Ser536-phosphorylation and IL-6 expression suggesting that RhoA was critical for Ang II induced RelA activation. Surprisingly, in VSMC there was no significant change in nuclear NF-κB abundance

during Ang II stimulation but there was increase accumulation of phosho-Ser536-RelA on the IL-6 promoter. In addition, IκBα levels were unperturbed. This suggests that Ang II activation of NF-κB is distinct from the canonical pathway in two ways: 1) IκBα degradation is not necessary for phospho-Ser536-RelA translocation and 2) only phospho-Ser536-RelA pool increases in the nucleus leading to gene transcription. Investigation of kinases regulating phosphorylation of Ser536 have demonstrated a role of IKKβ (16), ribosomal S6 kinase (RSK) and NF-κB inducing kinase [NIK; (17)] in activating NF-κB.

ANG II INDUCES AORTIC DISSECTIONS AND ANEURYSMS VIA IL-6 AND CCR2

IL-6 is a highly induced NF-κB dependent cytokine in vascular inflammation. High level of circulating IL-6 is associated with human AAA (18) and correlates with increased risk of aneurysm rupture (19). IL-6 is secreted by many vascular cells including macrophages, fibroblasts and VSMCs (20). To understand the role of IL-6 in the development of aortic dissections and AAA, Tieu BC et al., infused normolipidemic wild-type (WT) and IL-6-deficient (IL-6 -/-) mice with "high" dose of Ang II (2500 ng/kg/min) for 7-10 days (8). Ang II infusion increased aortic IL-6 secretion by 2-to 4-fold in WT mice. Immunohistochemistry (IHC) suggested that the source of IL-6 was in the adventitia-site of fibroblast and monocyte accumulation. Approximately 33% of the Ang II infused WT mice developed aortic dissections within the first 7 days whereas IL-6 -/- mice were completely protected. Infusion of Ang II for 10 days induced dissection in a small cohort of IL-6 -/- (12.5%) suggesting that IL-6 –deficiency delays the onset of aortic dissections. In addition, Ang II infusion promoted accumulation of monocytes/macrophages in WT aortas and their accumulation was significantly blunted in IL-6 -/- mice. To determine the role monocyte/macrophage in IL-6 secretion and aortic dissection, Ang II was infused into WT and CCR2 -/- animals. CCR2 is the chemokine receptor for MCP-1 and MCP-3, and is involved in monocyte recruitment to site of inflammation (21). It is also necessary for

monocyte extravasation from the bone marrow into circulation (21). CCR2-/- animals were protected from aortic dissections during the first week of Ang II infusion whereas a few developed dissection following 10 days of infusion. Interestingly, adoptive transfer of CCR2+/+ monocytes into CCR2-/- animals promoted an increase incidence of dissections (57.1%), and further strengthened the finding that monocyte recruitment to the aortic wall is crucial for Ang II induced dissections. Since, IL-6 and MCP-1 localized to the adventitia where fibroblasts and monocytes were also observed, in vitro co-cultures of aortic adventitial fibroblast and circulating monocytes were performed and cytokine secretions were measured. Co-culture of aortic fibroblast with monocytes induced a 2.5- to 3-fold increase in IL-6 even in the presence of an inset the prevented direct contact between the two cell types. Furthermore, IL-6 induced MCP-1 and matrix metalloproteinase-9 (MMP-9) production in monocytic cells. This suggested a mechanism which correlated with the *in vivo* data: Ang II induces monocyte recruitment to the aortic wall where monocyte-fibroblast interaction is important in IL-6 amplification; IL-6 activates monocytes into macrophages, induces chemokine and matrix destabilizing MMP-9 expression leading to aortic wall dissection. In a subsequent study, it was demonstrated that Ang II infusion induces aortic fibroblast proliferation in the adventitia (22). Furthermore, aortic fibroblasts *in vitro* secreted more IL-6 than any other cytokine surveyed and fibroblast- IL-6 was 300-fold more concentrated than IL-6 from THP-1 monocytic cells (22). These data suggested that aortic fibroblast is the primary producer of IL-6 and therefore is a critical cell involved in vascular inflammation. Since IL-6 is a RelA- dependent cytokine, it also suggested that aortic fibroblast-RelA is the key intracellular transcription factor that promotes vascular inflammation and aortic dissections.

In the first study presented here my aim was to explore the role of fibroblast-RelA in the development of Ang II induced vascular inflammation and AAA formation. As mentioned above, Ang II infusion leads to aortic dissection in the supra-renal aorta before aneurysm formation. To test my hypothesis that fibroblast-RelA was crucial for the

development of vascular inflammation and AAA, I planned to delete RelA from vascular fibroblasts using Cre-Lox technology before challenging the animals with Ang II. To achieve this aim, I helped develop a transgenic mouse harboring RelA alleles that contained loxP sites in intron 4 and intron 8. The RelA-flox (RelA f/f) mouse was mated with a mouse expressing Cre recombinase fused with modified estrogen receptor binding domain (ER^T) and driven by the Collagen 1α2-promoter (Col1a2-$CreER^T$) to generate a double transgenic (RelA f/f•Col1a2-$CreER^T$). Col1a2-$CreER^T$ is expressed in dermal, cardiac and vascular fibroblast (23). I planned to excise RelA exons 5-8 from vascular fibroblast in RelA f/f•Col1a2-$CreER^T$ mice using tamoxifen mediated $CreER^T$ activation. The recombined alleles would fail to express functional RelA mRNA transcripts leading to fibroblast-RelA deletion. To verify the specificity of Col1a2-$CreER^T$ activation, the Col1a2-$CreER^T$ mouse was first crossed with an mT/mG Cre-reporter mouse. In this mouse, cells contain a knocked-in allele in the ROSA26 locus that encodes for dimer Tomato (dTomato) red fluorescent protein targeted for the plasma membrane (mT) (24). *dTomato* is flanked by loxP sequences and is located upstream of enhanced green fluorescent protein (eGFP) allele. Cells containing the *mT/mG* allele continuously express dTomato. After Cre induction, *dTomato* allele is excised out and *eGFP* is expressed (mG) leading to a fluorescence color-switch from red to green that can be observed with fluorescence microscopy. The results from these experiments help define the specificity of the Col1a2-$CreER^T$ and also demonstrate the role of aortic wall -RelA in AAA formation.

DERMAL FIBROBLASTS MEDIATE WOUND HEALING AND FIBROSIS

Cutaneous wound healing is a multi-step process involving infiltration of leukocytes that clear cellular debris, formation of provisional matrix that guides infiltrating leukocytes and resident fibroblast, re-epithelization, and deposition of collagen fibers, which alongside myofibroblasts promote wound closure (25). Following burn injury, this process is often exaggerated with excessive deposition of extracellular matrix (ECM) that

results in a hypertrophic scar (HTS). These erythematous lesions are usually pruritic with a stiff and rough texture. The mature scar can be very problematic for patients causing compression, anatomic deformity and decrease joint mobility (26). Current treatments such as silicone gel sheeting and compression therapy provide slight benefit by mitigating the redness and thickness of the scar (27). Since these treatments are partially beneficial, there is a great need to better understand the molecular mechanisms involved in HTS formation which can be exploited to modify the repair process and prevent adverse outcomes following burn injury.

Myofibroblasts, which are present in limited number in normal skin, are found in overabundance in HTS after burn injury. These cells produce high levels of ECM proteins including collagen I (Col1) and 3 (Col3) and fibronectin (28). In addition, myofibroblasts express smooth muscle cell genes such as smooth muscle cell α- actin (αSMA) and actin associated SM22α (28). Accumulation of αSMA fibers provides contractile strength which can be measured with collagen gels. Although multiple sources contribute to myofibroblast population after injury including cells that undergo epithelial-to-mesenchymal transition and circulating leukocytes, resident dermal fibroblasts are likely the primary cells that transdifferentiate into myofibroblasts.

TGFβ is a potent and well-characterized cytokine that promotes myofibroblast transdifferentiation. This cytokine is upregulated after injury and is released from resident mesenchymal cells and circulating leukocytes. TGFβ1 binds to its receptor (TGFβRII) which heterodimerizes with TGFβRI, a serine-threonine kinase also known as ALK5, and phosphorylates it to initiate signal transduction (29). In the canonical pathway, the phosphorylated ALK5 receptor complex recruits and phosphorylates transcription factors Smad2 and Smad3. Phospho-Smad2/3 dimerize and complex with Smad4 before translocating to the nucleus to initiate gene transcription. The canonical signaling pathway is considered essential for myofibroblast transdifferentiation (28).

In lung and cardiac fibroblasts, TGFβ induces generation of reactive oxygen species (ROS) that mediates myofibroblast transdifferentiation. TGFβ specifically upregulates NADPH oxidase (Nox) 4 which utilizes electrons from NADPH to make superoxide before rapidly converting it to hydrogen peroxide (30). Unlike other members of Nox family of enzymes that are regulated by stimulus induced assembly of regulatory subunits (p47, p67 and Rac1), Nox4 is regulated mainly at the level of gene expression (31). Smad3 controls Nox4 expression by binding to a distal Smad binding element (SBE) on the Nox4 promoter (32). Suppression of Nox4 decreases myofibroblast formation and fibrosis in lung (31), liver (33), kidney and cardiac (34) injury models. In this study, we investigated whether dermal fibroblasts also utilize Nox4 to promote myofibroblast transdifferentiation and whether Nox4 generated ROS regulates most aspects of myofibroblast gene expression program.

Gene transcription is a multi-step process involving transcription initiation and transcription elongation. Inflammatory and infectious stimuli initiate signaling cascades spurring the binding of transcription factors such as nuclear factor-kappa B to specific DNA motifs and recruitment of RNA polymerase II (Pol II), which is phosphorylated at Ser5 on its C-terminal domain (CTD) to initiate transcription (35). Small transcripts of 30-60 nucleotides are transcribed until Pol II is phosphorylated on Ser2 and released from its pause site by positive-transcription elongation factor-b (P-TEFb), a complex of cyclin T1 and cyclin-dependent kinase 9 (CDK9) (35). Bromodomain and extraterminal domain (BET) containing protein BRD4 interacts with P-TEFb and blocks 7SK/HEXIM, a ribonucleoprotein complex that keeps P-TEFb in an inactive state, from associating with P-TEFb (36). Furthermore, BRD4 itself has kinase activity and can phosphorylate Pol II Ser2 to promote transcription elongation (37). In addition to investigating the role of Nox4 in dermal myofibroblast transdifferentiation, we sought to determine whether fibrotic gene program initiated by TGFβ requires CDK9 and BRD4 to promote Nox4 transcription and

whether these transcription co-activators have overlapping roles in regulating the myofibroblast genes.

Chapter 2: Angiotensin II Induces Vascular Inflammation and AAA Formation via Activation of Aortic-NF-κB/RelA Signaling

My first aim was to explore the role of fibroblast-RelA in mediating vascular inflammation and AAA in the Ang II infusion model. As part of this aim, I helped develop a RelA f/f transgenic. During the generation of this mouse, we mated a RelA f/+ mouse with a Zp3-Cre transgenic to obtain a whole-body RelA+/- female mouse. In the Zp3-Cre transgenic, the Cre expression is controlled by regulatory elements of the *zona pellucida 3* (*Zp3*) gene which is expressed exclusively in the growing oocytes. The ZP3-Cre mediated loxP recombination occurs in 100% of the oocytes (38). The RelA+/- female was backcrossed with a C57Bl/6 male to propagate the knockout (KO) allele. Mating of a RelA+/- male and RelA+/- female mouse produced only RelA+/+ and RelA+/- mice. Analysis of embryos at embryonic day 12 (E12) demonstrated that almost a quarter of them had intraabdominal hemorrhages and no macroscopic discernment of a liver (Figure 1A). Genotyping verified that these embryos were RelA-/-. Furthermore, mouse embryonic

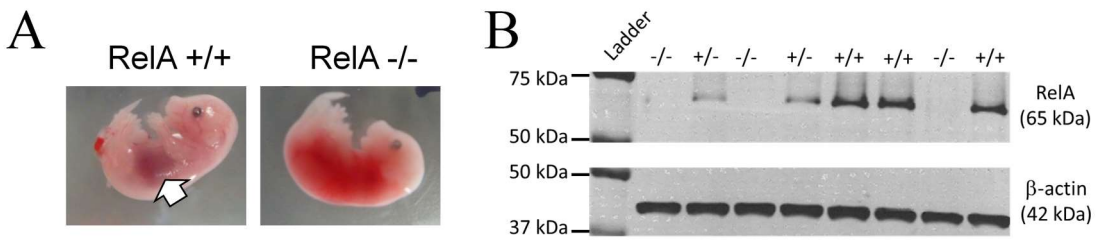

Figure 1: Whole body RelA-deficiency leads to intraabdominal hemorrhage and embryonic lethality.

A) Embryos isolated at embryonic day 12 (E12) exhibited presence of a liver in RelA+/+ (white arrow), which was absent in the RelA-/-. B) Mouse embryonic fibroblasts (MEFs) were propagated in cell culture and Western blot was performed on passage 2 cells. Immunoblotting for RelA demonstrated that RelA was diminished in RelA+/- cells and completely absent in RelA-/- cells.

fibroblasts (MEFs) were isolated to verify RelA protein depletion in RelA-/- cells (Figure 1B).

These experiments confirmed an observation fist made by Beg *et al*. that whole-body RelA-deficiency leads to embryonic lethality due to an inability of the embryo to develop a functioning liver (39). In addition, absence of RelA protein in RelA-/- MEFs suggested that the RelA-flox allele, which was used to generate the KO, is able to undergo Cre-mediated recombination to form a RelA-null allele.

ANG II ACTIVATES NF-ΚB/RELA SIGNALING IN THE AORTIC WALL

Ang II is a potent inducer of RelA-dependent cytokine IL-6 *in vivo* and *in vitro* (12). Furthermore, Ang II infusion into rats increases total aortic phospho-Ser536-RelA as measured by ELISA assay (15). To find out which aortic cells have increased RelA-signaling during Ang II infusion, we infused n= 3 WT mice with saline (sham) and n= 4 WT mice with Ang II at a rate of 2500 ng/kg/min for 7 days before isolating their aortas for IHC and qRT-PCR analysis. None of the animals developed an aortic aneurysm over the one week period. In IHC analysis of supra-renal abdominal aortas, there was dramatic increase in phospho-Ser536-RelA signal in aortas from Ang II infused mice verifying that Ang II is a potent inducer of RelA-signaling in the aortic wall (Figure 2A). Furthermore, Ang II induced phospho-Ser536-RelA formation abundantly throughout the media and the expanded adventitia suggesting that Ang II activates RelA-signaling in multiple cell-types. Since IL-6 is a downstream target of phospho-Ser536-RelA, we performed immunofluorescence analysis for IL-6 in both groups. There was some positive immunostaining for IL-6 in aortas from the sham group but increased immunostaining was observed in the media and the adventitia in aortas from the Ang II group (Figure 2A, bottom panel). These data sets complement each other and support the conclusion that Ang II activates phospho-Ser536-RelA signaling in medial and adventitial cells of the abdominal aorta.

Next, we wanted to verify the identity of the cells in the medial and adventitial layers. VSMCs populate the media and express high levels of smooth muscle cell α-actin (αSMA). Immunofluorescence detection of αSMA via confocal microscopy verified that medial cells were αSMA+ (Figure 2B). In addition, there was almost complete absence of αSMA signal in the adventitia, with very few adventitial cells expressing some signal above background. This verified that majority of the medial cells were αSMA+ VSMCs, although myofibroblasts are also known to express αSMA and may be present in the medial and adventitial layers. Platelet derived growth factor α (PDGFRα) is found on Col1α1-expressing cells in the myocardium and was demonstrated to be a reliable marker for cardiac fibroblasts (40). Detection of PDGFRα in the aortic wall via immunofluorescence

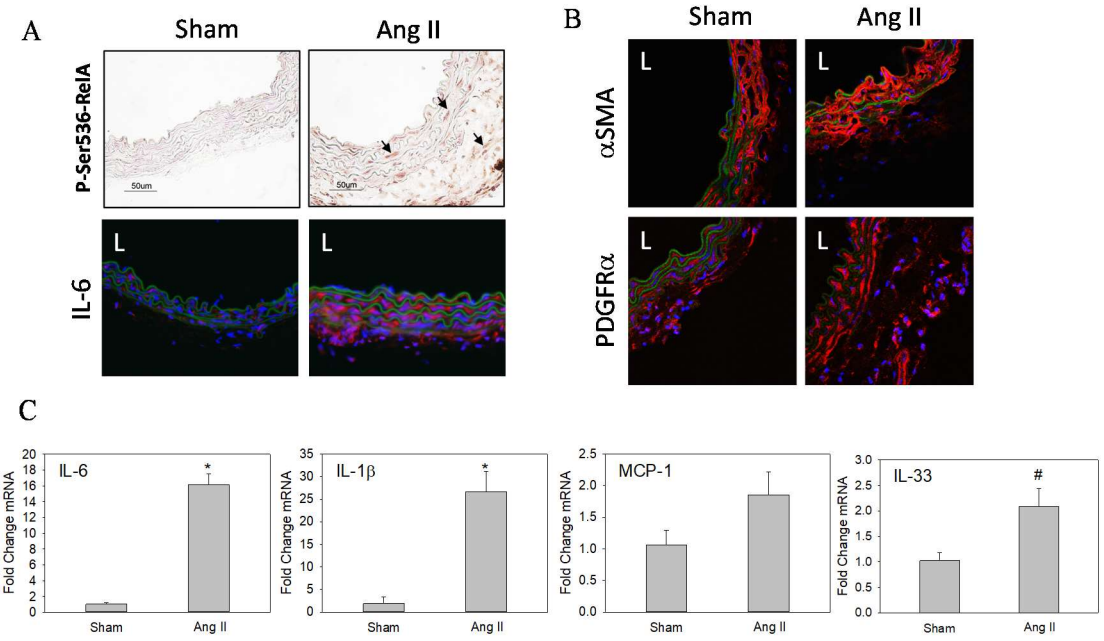

Figure 2: Ang II stimulates RelA activity in the aortic wall.

A) IHC for phospho-Ser536-RelA and IL-6 in abdominal aortas from sham and Ang II infused mice. Black arrows indicate positive staining. B) Immunofluorescence detection of αSMA and PDGFRα via confocal microscopy in abdominal aortas. L indicates vessel lumen. C) Quantitative- reverse transcriptase- PCR analysis of RelA dependent genes in the aorta. Data is presented as mean ± SEM. *P< 0.05; # P= 0.055.

suggested that it is found on cells of the media and the adventitia with no specificity for adventitial fibroblasts (Figure 2B).

In addition to mediating the transcription of IL-6, RelA is involved in transcription regulation of multiple other cytokines/chemokines including IL-1β, MCP-1 and IL-33. QRT-PCR analysis was performed on aortas from sham and Ang II group to determine the relative mRNA abundance of these chemokines/cytokines. Ang II infusion dramatically increased IL-6 transcripts by 16-fold and IL-1β transcripts by approximately 25-fold (Figure 2C). Furthermore, IL-33, a member of IL-1 family of cytokines was increased by 2-fold. Although the chemokine MCP-1 was slightly elevated in aortas from the Ang II group, 1.8-fold vs. sham, the difference was not significant. Elevation of IL-6, IL-1β and IL-33 transcripts further validate the IHC experiments and verify that Ang II infusion stimulates RelA-signaling in the aortic wall.

CHARACTERIZATION OF COL1a2-CREER^T MICE

To test my hypothesis that fibroblast-RelA is important in vascular inflammation and AAA formation, I planned to generate fibroblast-specific RelA-deficient mice by tamoxifen mediated Cre recombination in RelA f/f•Col1a2-CreER^T transgenic. In addition to mating the Col1a2-CreER^T mice with RelA f/f mice to generate the necessary double transgenic, I crossed the Col1a2-CreER^T mice with mT/mG Cre-reporter mice to determine the specificity of Col1a2-CreER^T activation.

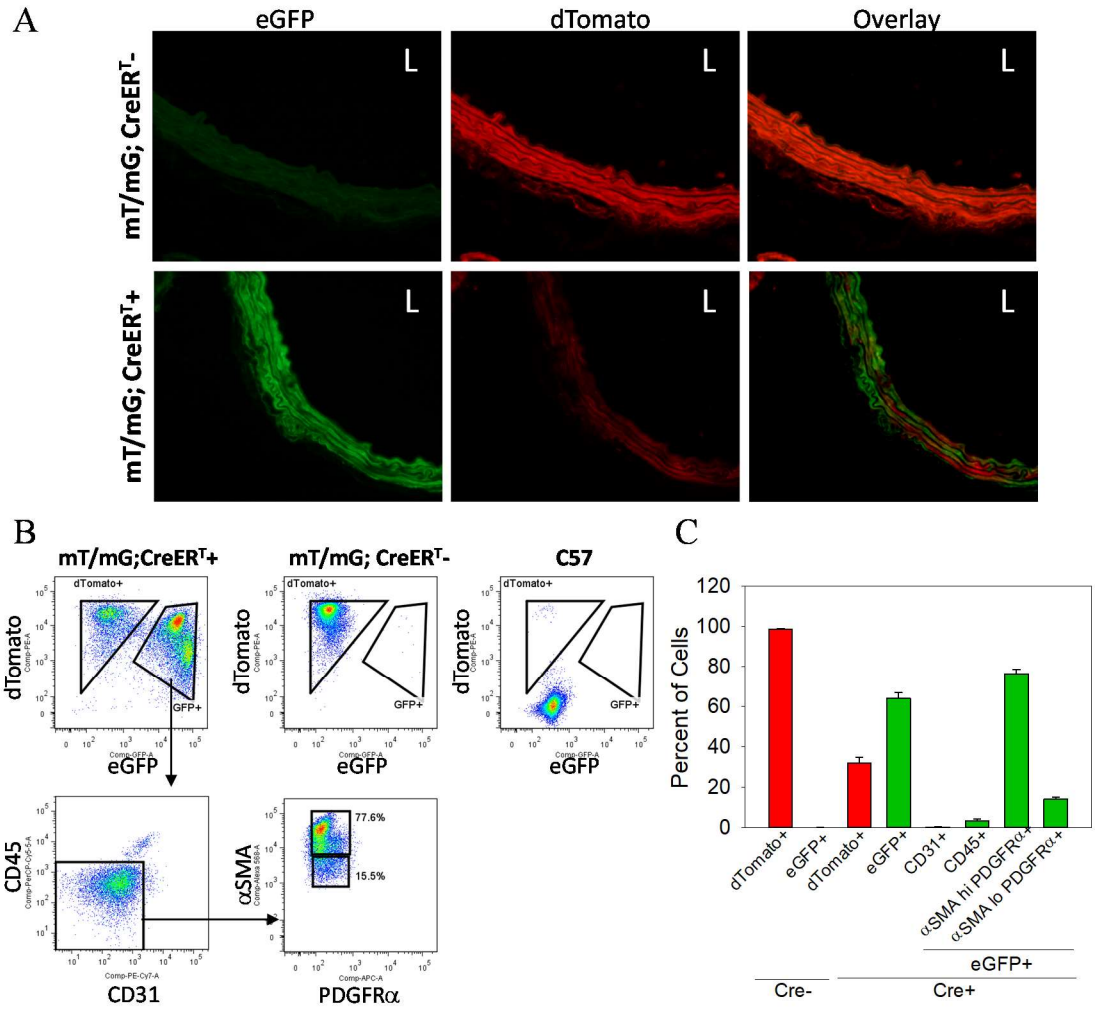

Figure 3: Tamoxifen activates Col1a2-CreER^T in aortic VSMCs and fibroblasts.

mT/mG•Col1a2-CreER^T + (n=5), mT/mG•Col1a2-CreER^T – (n=5) and C57Bl/6 (n=2) mice were treated with tamoxifen for 10 days. Aortas were collected after a 2-week period and analyzed via A) fluorescence microscopy or B) flow cytometry. L indicates vessel lumen. Flow cytometric data is presented as mean ± SEM.

Adult mice, mT/mG•Col1a2-CreER^T + or mT/mG•Col1a2-CreER^T - were given intraperitoneal (IP) injections of tamoxifen for 10 consecutive days. After a 2-week period to ensure sufficient recombination had occurred, aortas were isolated for characterization via fluorescence microscopy and flow cytometry. Abdominal aortas from Col1a2-CreER^T- mice expressed only red fluorescence indicating that no recombination had taken place

(Figure 3A). In contrast, aortas from Col1a2-CreER^T + mice expressed green and red fluorescence, but surprisingly, the green fluorescence emanated from cells throughout the medial and adventitial layers. To determine exactly which cells undergo recombination with tamoxifen activation of Col1a2-CreER^T, aortic cells were dissociated into single cell suspension and labeled with fluorochrome conjugated antibodies for flow cytometric analysis (Figure 3B). Tamoxifen induced approximately 60% of the aortic cells in Col1a2-CreER^T + mice to undergo recombination and express eGFP (Figure 3C). There were negligible amount of eGFP+ cells that expressed CD31 (<1%), endothelial cell marker, and less than 5% expressed CD45, the leukocyte marker. Majority of the eGFP+ cells were PDGFRα+αSMA^{hi} (~80%) and PDGFRα+αSMA^{lo} (~ 15%). I classified PDGFRα+αSMA^{hi} as VSMCs and PDGFRα+αSMA^{lo} as aortic fibroblasts since immunofluorescence staining for αSMA previously suggested that majority of the medial VSMCs express high levels of αSMA, whereas adventitial fibroblasts expressed very minute amount of this protein.

VERIFICATION OF TAMOXIFEN INDUCIBLE RELA-DEFICIENCY IN COL1a2-CREER^T MICE

Although Col1a2-CreER^T mediated recombination occurs in fibroblasts and VSMCs, I decided to continue experimentation with this mouse because I found RelA-signaling to be triggered in both cell-types during Ang II infusion (Figure 2). Therefore, RelA f/f•Col1a2-CreER^T + and RelA f/f•Col1a2-CreER^T – mice were treated with tamoxifen to generate aortic wall- RelA-/- and -RelA+/+ mice, respectively. Flow cytometry analysis of VSMCs indicated that RelA median fluorescence intensity (MFI) decreased by almost 40% in RelA-/- mice (Figure 4A). Furthermore, RelA MFI in aortic fibroblast diminished by more than 60% in RelA -/-. To confirm that RelA was being depleted in VSMCs and aortic adventitial fibroblasts, IHC for RelA was performed on abdominal aortic cross-sections. Immunofluorescence signal for RelA was very robust in

RelA +/+ aortas whereas a significant reduction in RelA signal was observed in the media and adventitia of the RelA-/- (Figure 4B). Lastly, qRT-PCR analysis was preformed to determine differences in RelA mRNA level (Figure 4C). In RelA-/- aortas, there was a 60% reduction in RelA mRNA transcripts and a similar level of reduction was observed in transcripts of A20, a RelA dependent gene. These experiments demonstrate that RelA can be significantly depleted in aortic fibroblasts and VSMCs using the Col1a2-CreER^{T}.

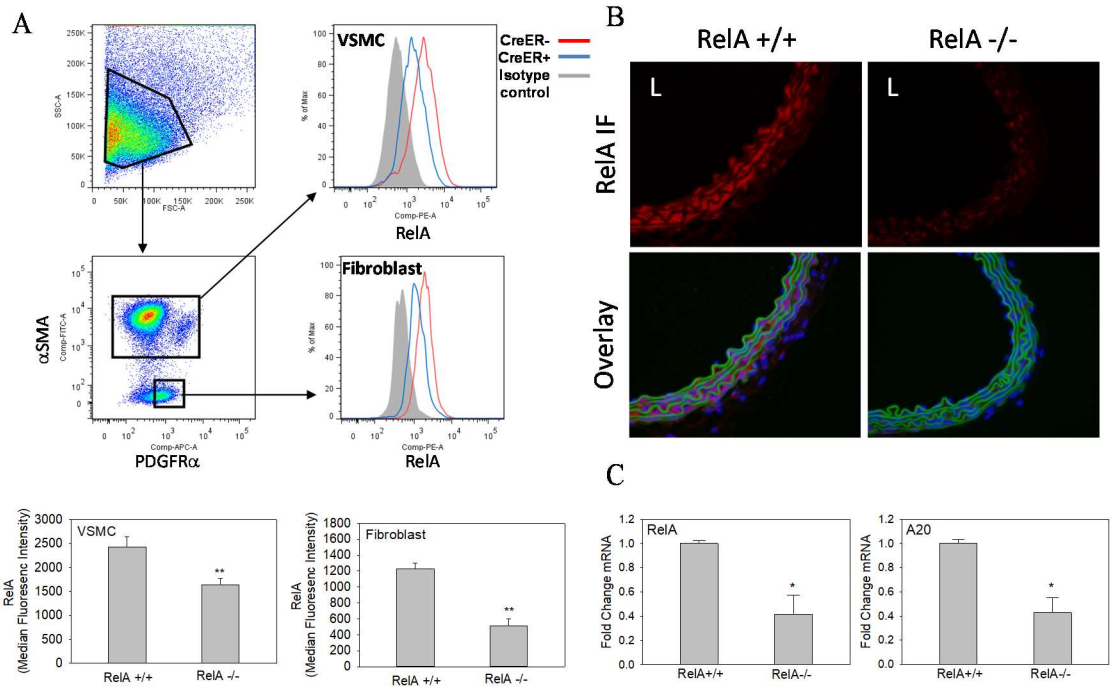

Figure 4: Verification of tamoxifen mediated RelA knockdown in RelA f/f•Col1a2-CreER^T mice.

RelA f/f•Col1a2-CreER^T + (n=8) and RelA f/f•Col1a2-CreER^T – (n=8) mice were treated with tamoxifen for 10 days. After a 3-week period, aortas were isolated for characterization via flow cytometry, IHC, and qRT-PCR. A) Flow cytometric analysis of RelA content in aortic VSMCs and fibroblasts. Bars represent the mean ± SEM of median fluorescence intensity from n= 4 aortas in each group. B) Immunofluorescence (IF) analysis of RelA in abdominal aortas from RelA+/+ and RelA-/- mice. C) qRT-PCR for RelA and RelA dependent gene, A20, was performed on aortas from RelA+/+ and RelA-/-. Bars represent mean ± SEM. ** and * P< 0.05 vs. RelA+/+.

RELA DEFICIENCY IN COL1a2-CREER^T MICE PROTECTS FROM ANG II-INDUCED AAA

Since I was able to attain significant depletion of RelA in VSMCs and aortic fibroblasts of RelA f/f•Col1a2-CreER^T + mice, I further investigated whether RelA depletion in these cell-types protects from the development of Ang II induced AAAs. In humans, AAA is defined as a 50% increase in the aortic diameter of the abdominal aorta. Aortic dilation in AAA is permanent and could prove fatal if the aortic wall is not re-enforced with a graft to limit the dilation. In the Ang II model of murine AAA, a hematoma with a bulbous deformity of the aortic wall is present that can be discerned by gross examination or via inspection under a dissecting scope. In my experiments, I used both

ultrasonography measurement of aortic diameter and/or analysis under a dissecting scope to determine the incidence of the disease.

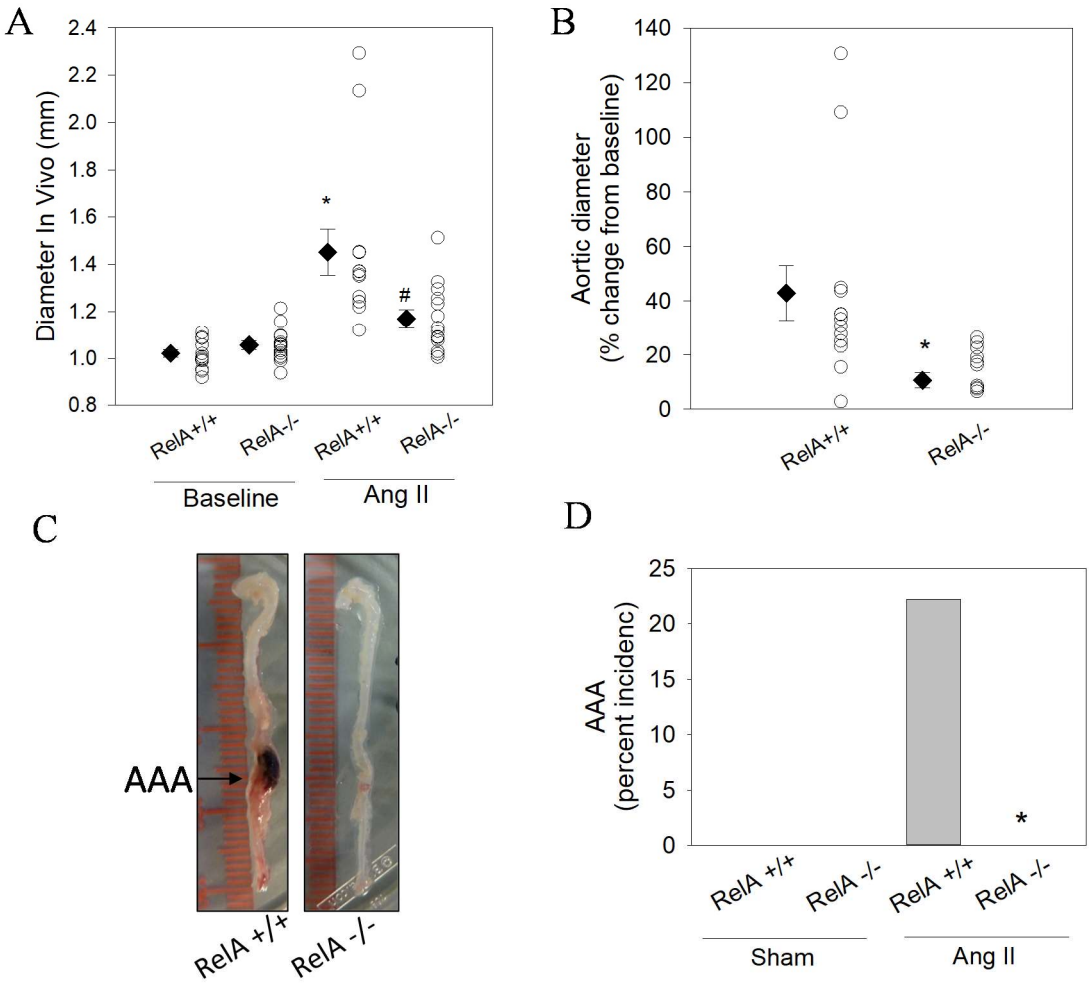

Figure 5: Ang II induces AAAs in aortic wall-RelA +/+ but not in aortic wall- RelA -/- mice.

Tamoxifen was use to induce RelA-deficiency in the aortic walls of RelA f/f•Col1a2-CreER^{T} + mice. Ang II was infused in aortic wall-RelA+/+ (n= 13) and -RelA-/- (n= 14) mice for 7 days. A) Abdominal aortic dimeters were measured at baseline and at day 6 of Ang II infusion. B) Change in aortic diameter as percent change from baseline. C) Images of representative aorta with AAA in RelA +/+ group and an aorta from RelA-/- group. D) Cumulative percent incidence of AAA determined from three separate experiments. Each circle represents measurement from a single animal. Diamonds with error bars represent the mean ± SEM of each group. *P< 0.05.

Aortic wall- RelA+/+ and RelA-/- were generated by tamoxifen administration to RelA f/f•Col1a2-CreER^{T}- and RelA f/f•Col1a2-CreER^{T} +, respectively. Three weeks after the last tamoxifen injections, baseline ultrasound measurements of the abdominal aorta were recorded before infusion of Ang II for 7 days. At day 6, ultrasound was used to measure changes in abdominal aortic diameter that may have occurred due to Ang II (Figure 5A). The mean aortic diameter of RelA+/+ significantly increased from 1.02 ± 0.017 mm at baseline to 1.45 ± 0.09 mm at day 6 of Ang II infusion. Interestingly, the mean aortic dimeter in RelA-/- at baseline (1.06 ± 0.019 mm) was not very different from the measurement at day 6 (1.17 ± 0.04 mm). Evaluation of diameter changes as percent change from baseline revealed that Ang II infusion increased the mean abdominal aortic diameter in RelA+/+ by 42.9% and in RelA-/- by only 10.6% (Figure 5B). There were few mice in the RelA+/+ group that developed a full blown AAA but mice in RelA-/- group remained protected from the disease. A representative image of the AAA is provided in Figure 5C. Cumulative incidence of AAA was determined from combining data from three separate experiments. These data indicated that 22.5% (4/18) of RelA+/+ mice developed AAA whereas there was a complete absence AAA in RelA-/- mice (0%, 0/19). Aortic cross-sections from RelA+/+ indicated presence of adventitial expansion and hematoma, changes which were absent in RelA -/- mice (Figure 6). Collectively, I interpreted this to mean that RelA-deficiency in aortic VSMCs and fibroblasts protects from Ang II induced aortic dilation, aortic wall remodeling and AAA development.

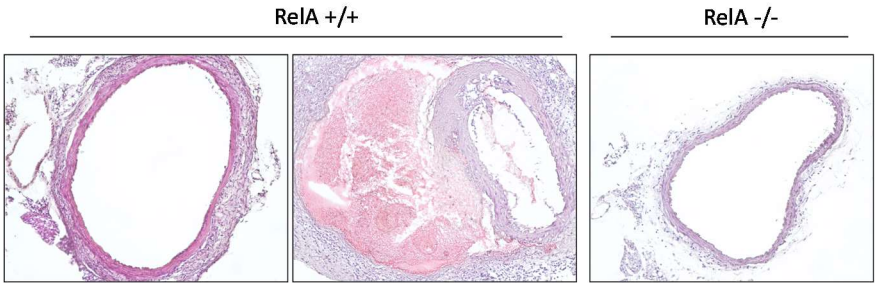

Figure 6: Aortic wall- RelA-/- are protected from adventitial remodeling and hematoma.

Representative images of H&E stained aortic cross-sections of abdominal aortas from RelA+/+ and RelA-/- mice infused with Ang II for 7 days.

DEFICIENCY OF RELA IN COL1A2-CREER^T MICE DECREASES AORTIC INFLAMMATION AND ADVENTITIAL EXPANSION

After observing that aortic wall-RelA deficiency protected mice from AAA, I investigated whether this was due to decrease production aortic cytokines. RNA was extracted from the aortas of aortic wall-RelA +/+ and -RelA-/- mice infused with Ang II for 7 days and subjected to qRT-PCR analysis. Aortas that developed AAAs were excluded from this analysis because I knew from past experience that AAAs overwhelming express high levels of cytokines and would eschew the data to one side. Aortic wall- RelA-/- aortas had a greater than 60% reduction in IL-6 mRNA abundance and almost a 75% reduction in IL-1β mRNA transcripts (Figure 7A). I also confirmed that RelA mRNA abundance was decreased in RelA-/- aortas by approximately 60% relative to RelA+/+ aortas. To further verify that IL-6 was decreased in the aortic wall of RelA-/- animals, I performed IHC on aortic cross-sections from the abdominal aortas. IL-6 immunofluorescence signal appeared bright throughout the aortic adventitia and was present in the media of RelA+/+ but highly diminished in RelA-/- (Figure 7B). Since Ang II and IL-6 induce MCP-1, the chemokine important for monocyte recruitment to the aorta, I performed IHC analysis to determine if there was any qualitative difference in MCP-1 expression between the two groups. Similar to IL-6, MCP-1 was abundantly present in the adventitia of RelA+/+ mice but there was

reduced presence in RelA-/- aortas (Figure 7B). During histological examination, I further observed that RelA+/+ aortas had thickened adventitia compared to RelA-/- aortas. To verify this observation, I quantified the adventitial area in H&E stained cross-sections using ImageJ software. Indeed, RelA-/- aortas from Ang II infused mice had significantly reduced adventitial area (0.122 ± 0.026 mm^2 vs. 0.041 ± 0.005 mm^2, RelA +/+ vs. RelA-/- ; Figure 7C). These data suggest that aortic wall-RelA deficiency protects from Ang II induced production of aortic cytokines thereby limiting vascular inflammation. In addition, decrease in aortic cytokines prevents the fibrotic adventitial expansion that accompanies vascular inflammation (22).

KNOCK-DOWN OF RELA IN COL1A2-CREER^T MICE DECREASES RECRUITMENT OF INFLAMMATORY MONOCYTES BUT DOES NOT AFFECT BLOOD PRESSURE

Since hypertension is a known risk factor for aortic dissections and Ang II is a known vasopressor, it was a possibility that the protective effect of RelA-deficiency in the aortic wall may be due to a decrease in blood pressure (BP). To test this hypothesis, aortic wall- RelA+/+ and RelA-/- mice were infused with sham or Ang II for 7 days. Baseline BP measurements were recorded for 4 consecutive days via the tail cuff method before pump implantation. In addition, BP was monitored for 4 consecutive days during Ang II infusion. Animals across all groups had similar starting body weights (Table 1). Furthermore, Ang II induced a slight induction in systolic BP in RelA +/+ compared to sham infused- RelA +/+ mice (Table 1). A similar vasopressor effect was observed in RelA-/- animals. In addition, Ang II induced elevation of heart rate in RelA+/+ and RelA-/- to similar extent. These data indicate that aortic-RelA deficiency does not affect Ang II induced hypertension.

Treatment	Sham		Ang II	
Genotype	RelA+/+	RelA-/-	RelA+/+	RelA-/-
N	3	3	5	5
Baseline Body weight (g)	21.6 ± 2	25.1 ± 1.8	23.3 ± 1.7	23.6 ± 1.4
Systolic BP (mmHg)	106.7 ± 2	111.1 ± 9	120.6 ± 8	135 ± 5
Heart rate (bpm)	689.9 ± 35	764.5 ± 58	1037.4 ± 92*	1102.0 ± 44*

Table 1: Ang II mediated effects on BP and heart rate.

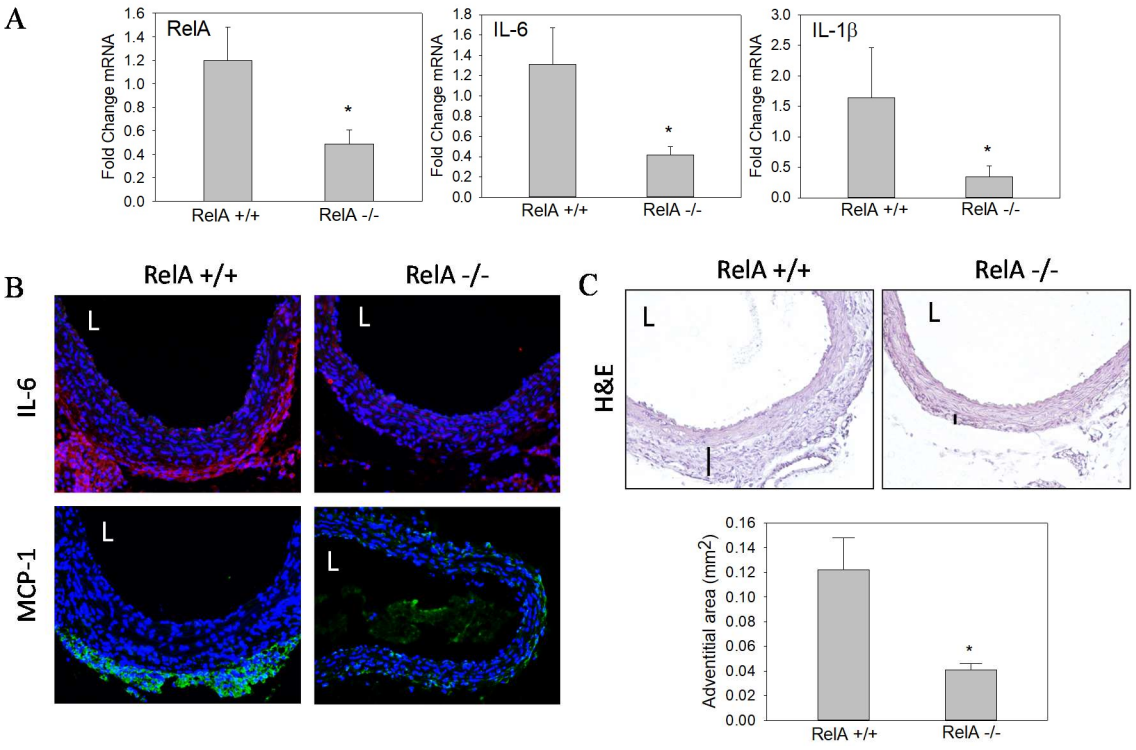

Figure 7: Aortic cytokine analysis in Ang II-infused mice.

A) qRT-PCR analysis of aortic RelA and aortic cytokines in RelA+/+ and RelA-/- mice infused with Ang II for 7 days. B) Immunofluorescence analysis of IL-6 and MCP-1. AF568-conjugated secondary antibody was used for detection of IL-6 (red signal) and AF488-conjugated secondary antibody was used for detection of MCP-1 (green signal). C) H&E stained aortic cross-sections were used to quantify the adventitial area. Black vertical lines indicate the extent of adventitial expansion in representative images. All data is presented as mean ± SEM. *P< 0.05.

To determine whether the aortic wall-RelA-/- mice are protected from AAA due to a difference in monocyte recruitment to the aorta, aortas were isolated at the termination of the blood pressure experiment for monocyte analysis via flow cytometry (Figure 8). To identify inflammatory monocytes, cells that were lineage-positive were excluded. Lineage refers to cells expressing CD90, B220, CD49b, NK1.1 or Ly6G. CD11b+Lin-negative cells were further divided into F4/80 hi/lo and Ly6C hi/lo subgroups. $F4/80^{lo}$ $Ly6C^{hi}$ cells have previously been demonstrated to be the inflammatory subset of monocytes that expresses high levels of CCR2 and are involved in cardiac inflammation following myocardial infarction. I found that Ang II dramatically increased $F4/80^{hi}Ly6C^{lo}$ macrophages and $F4/80^{lo}Ly6C^{hi}$ monocytes in RelA+/+ aortas (37% of CD11b+Lin- cells). Furthermore, RelA-/- aortas had very little accumulation of $F4/80^{lo}Ly6C^{hi}$ monocytes (2-4% of CD11b+Lin- cells), although $F4/80^{hi}Ly6C^{lo}$ macrophage accumulation still occurred. This suggests that aortic wall-RelA deficiency prevents Ang II induced recruitment of inflammatory monocytes. Decrease in monocyte recruitment is likely one important mechanism that explains the prevention of AAA in aortic wall-RelA-/- animals.

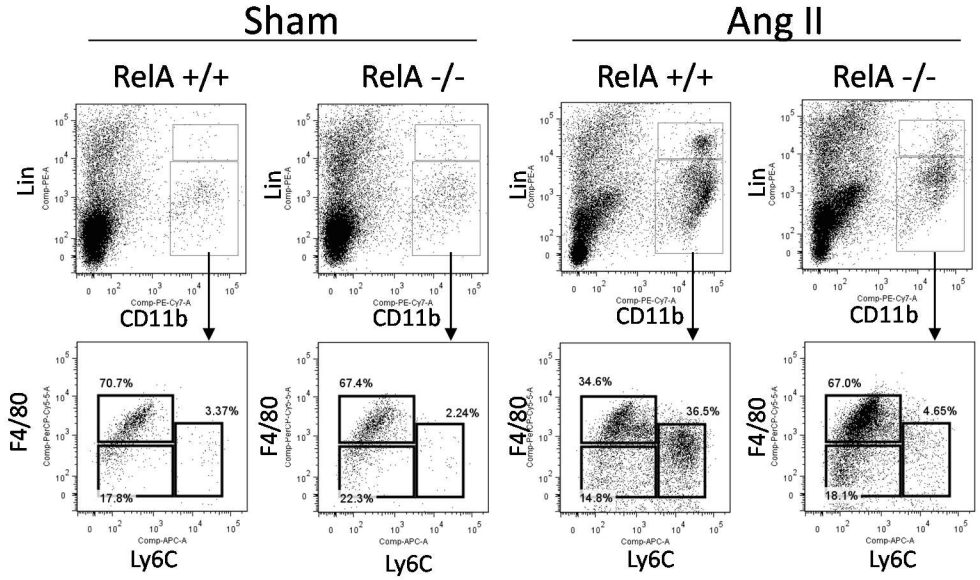

Figure 8: Flow cytometric analysis of aortic monocyte and macrophages in aortic wall- RelA+/+ and –RelA-/-.

Lin represents lineage markers CD90, B220, NK1.1, CD49b and Ly6G.

SUMMARY AND DISCUSSION

In the work presented above, I demonstrate that I was able to successfully develop a RelA f/f mouse that can be crossed with a Cre-transgenic to generate cell-specific RelA-KO. The use of Cre-Lox technology allowed me to bypass a major limitation that accompanies whole-body RelA deficiency- death in utero. My original hypothesis was that fibroblast-RelA plays a critical role in Ang II induced vascular inflammation and AAA formation. To test this hypothesis I planned to use the Col1a2-CreER^T mouse, a transgenic line in which tamoxifen mediated recombination was previously demonstrated to occur in fibroblasts including those in the adventitia of the vasculature. My experiments with mT/mG•Col1a2-CreER^T mice indicated that tamoxifen induces Col1a2-CreER^T activity in both VSMCs and aortic fibroblasts. Since Ang II induced phosph-Ser536-RelA signaling in both of these cell-types, I continue forward with my planned experiments with Col1a2-

$CreER^T$ transgenic. My results suggest that RelA deficiency in aortic cells (VSMCs and fibroblasts) protects from Ang II induced aortic dilation and AAA formation. Furthermore, aortic wall- RelA-/- aortas expressed less amount of potent inflammatory cytokines IL-6 and IL-1β and their adventitial expansion was significantly limited. Flow cytometry analysis suggested that aortic wall-RelA was also important in mediating the recruitment of inflammatory $F4/80^{lo}Ly6C^{hi}$ monocytes since aortic wall-RelA-/- animals had very little accumulation of this monocyte subset in the aorta. Furthermore, I found that the protective effects of aortic wall- RelA-/- were independent of Ang II pressor effect since there was modest elevation of blood in both RelA+/+ and RelA-/- animals during Ang II infusion.

Although there were some interesting results that come from this study, several questions remained to be answered. First, it still unknown whether its aortic fibroblast-RelA or VSMC-RelA that is more important in mediating vascular inflammation. Furthermore, several kinases are known to activate RelA via phosphorylation of Ser536 *in vitro*. It remains to be determined which kinase is important in mediating Ang II's inflammatory effects *in vivo*. Although aortic wall-RelA-/- aortas had decreased accumulation of inflammatory monocyte, $F4/80^{hi}Ly6C^{lo}$ macrophage accumulation still occurred. The role of inflammatory monocytes versus macrophage accumulation in the aortic wall during AAA formation also remains to be further defined.

The complete study describing this work was published in the journal of *Arteriosclerosis, Thrombosis and Vascular Biology* (41).

Chapter 3: TGFβ-Smad3 Signaling Requires BRD4 and CDK9 to Regulate Nox4 Expression and Promote Myofibroblast Transdifferentiation

In addition to investigating the role of fibroblast- RelA in development of AAA in vivo, I delved further into the mechanism of fibroblast phenotype changes that occur during injury and repair. Fibroblast to myofibroblast transdifferentiation during the healing process leads to secretion of increased amounts of ECM proteins and generation of contractile strength via expression of intracellular SMC associated genes such as αSMA. We observed the presence of αSMA+ cells in the adventitia of WT mice infused with Ang II but the underlying mechanism that promoted the development of myofibroblast and the significance of these cells in the aortic wall remained to be explored. Cellular culture experiments utilizing human aortic adventitial fibroblasts were extremely difficult to replicate as the cells underwent senescence within 4 passages. Therefore, I utilized human dermal fibroblast, which had a greater mitotic capacity to explore the mechanisms that promote fibroblast to myofibroblast transformation and found a relevant link of this process in hypertrophic scare formation in patients with burn injury.

TGFβ Promotes Dermal Fibroblast Nox4 Expression and Myofibroblast Transdifferentiation.

To determine the extent of myofibroblast population in non-burn skin (NBS) and in HTS, we performed immunofluorescence staining for αSMA on skin biopsies of patients taken 12-48 months following burn injury (Figure 9A). αSMA is considered the most reliable marker for myofibroblasts and therefore was utilized throughout this study as the myofibroblast differentiating marker. Immunofluorescence data indicated that

myofibroblasts are highly abundant in the deep dermal layer of HTS at 12-24 months but disappear by 48 months after injury. In contrast, very few, if any, myofibroblasts were present in the NBS biopsies. We asked whether these myofibroblasts also produced TGFβ, the key cytokine that promotes their contractile and hypersecretory state. Immunohistochemistry for TGFβ on serial sections from the same biopsy samples (Figure 9B) demonstrated robust staining in cells of the deep dermis, the same location where we observed most amount of αSMA+ staining, at 12-24 months suggesting that the myofibroblasts themselves were a major producer of TGFβ in HTS. Human dermal fibroblasts (hDF) were then stimulated with TGFβ *in vitro* up to 48h to determine changes in expression of Nox4 and other myofibroblast genes (Figure 9C). Sm22α increased steadily and peaked at 48h (40.3-fold increase vs. 0h), whereas Nox4 expression peaked at 12h (138-fold increase vs. 0h) followed by a gradual decline to 48h. Fibronectin (5.3-fold increase vs. 0h) and Col1α1 expression (3.3-fold increase vs. 0h) also increased over the same time-frame. These data suggested that hDF rapidly upregulates Nox4, SM22α and ECM genes fibronectin and Col1α1 when exposed to TGFβ, similar to lung and cardiac fibroblasts. Since the development of αSMA+ fibers is the hallmark of myofibroblasts, we performed immunofluorescence staining for αSMA with AF-488 conjugated secondary antibody and fluorescent staining for filamentous actin with AF-568 conjugated phalloidin, after stimulating the cells with TGFβ in the presence or absence of an ALK5 inhibitor (Figure 9D). By 24h, ~30% of the cells had developed αSMA+ fibers and ~50% had αSMA+ fibers by 48h. In addition, ALK5i completely blocked αSMA+ fiber formation. We performed Western blot analysis on hDF lysates after 24h following the same treatments (Figure 9E). Presence of ALK5i blocked TGFβ-induced phospho-Smad2/3 induction and de-novo αSMA formation. We interpreted these results to mean that 1) vast majority of hDF cells are mostly quiescent fibroblasts and have not transdifferentiated in culture to myofibroblasts in absence of TGFβ; 2) hDF cells could be used as a model to study myofibroblast transdifferentiation; 3) TGFβ induces myofibroblast

transdifferentiation via ALK5 mediated phospho-Smad2/3 activation; and 4) hDF cells also upregulate Nox4 rapidly after TGFβ exposure suggesting that Nox4 may be pivotal to controlling myofibroblast transdifferentiation program in hDF cells.

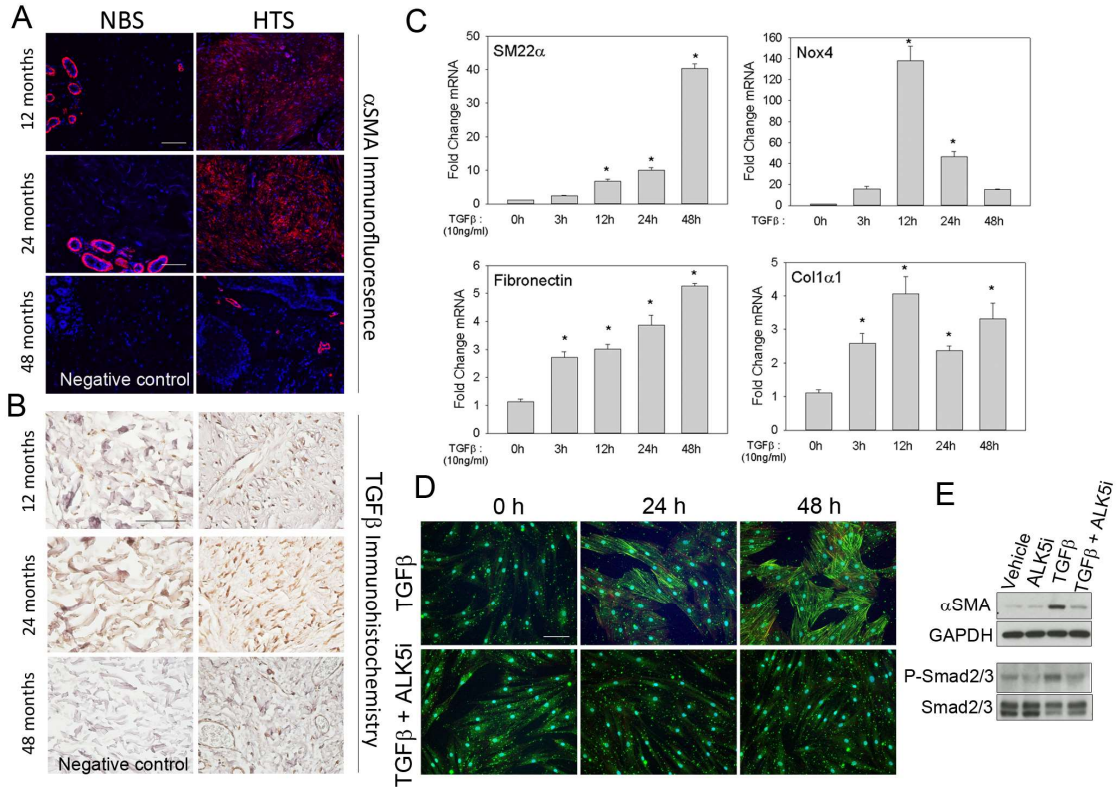

Figure 9: TGFβ induces dermal fibroblast Nox4 expression and promotes transdifferentiation to myofibroblast**.**

A) Immunofluorescence detection of αSMA+ myofibroblasts in skin biopsies taken from burn patients, 12-48 months after injury, at the site of hypertrophic scar (HTS) formation and from the adjacent non-burn skin (NBS). Positive staining for αSMA is in red and counterstaining for nuclei is in blue. Scale bar represents 100 microns. B) Immunohistochemistry for TGFβ in HTS and NBS tissue sections from burn patients. Positive staining for TGFβ is brown and counterstaining for nuclei is blue. Scale bar represents 100 microns. C) Human dermal fibroblasts (hDF) were stimulated with TGFβ (10 ng/ml) for 0-48 h and changes in gene expression for SM22α, Nox4, fibronectin and Col1α1 were analyzed via quantitative real-time PCR (qRT-PCR). Gene expression was normalized to DNA polymerase β mRNA. Data is presented as mean ± SEM. This experiment was repeated three times. * $P < 0.05$ vs. 0 h. D) hDF cells were seeded on coverslips, pre-treated with 10 μM ALK5i, LY2157299, before being stimulated with TGFβ (10 ng/ml) for up to 48 h. Immunostaining for αSMA (green) and staining for filamentous actin using phalloidin (red) was performed. αSMA+ cells (green or yellow fibers) were considered to be myofibroblasts. Scale bar represents 100 microns. E) hDF cells were pre-treated with vehicle or 10 μM ALK5i and then stimulated with TGFβ (10 ng/ml). Whole cell extracts were collected after 24 h and Western blot analysis was performed to analyze de-novo αSMA production and phospho-Smad2/3. GAPDH and Smad2/3 served as loading controls.

NOX4 INHIBITION WITH GKT137831 OR DEPLETION WITH SIRNA INHIBITS MYOFIBROBLAST DIFFERENTIATION WITH LIMITED EFFECT ON MYOFIBROBLAST GENES.

Since Nox4 is highly expressed within 3h of TGFβ exposure and precedes the maximum induction of SM22α, fibronectin and Col1α1, we asked whether inhibition of Nox4 with a small molecule inhibitor GKT137831 prevent myofibroblast transdifferentiation and induction of myofibroblast genes. Stimulation of hDF with TGFβ for 48 hours increased αSMA+ myofibroblasts from 0.77 % to 42.6 % of total cells, which was reduced to 13.2 % of cells with 20 μM GKT137831 pre-treatment (Figure 10A). Surprisingly, analysis of myofibroblast gene expression changes indicated that TGFβ induced increases in SM22a, Nox4 and fibronectin were unaltered by GKT137831 treatment whereas there was a slight reduction in Col1α1 with GKT137831 (5.1 ± 0.4 vs. 3.8 ± 0.3 fold change, TGFβ vs. TGFβ + GKT137831; Figure 10B). An essential aspect of a myofibroblast is its ability to generate force for contraction, which can be assayed by measuring changes in surface area of collagen gels. GKT137831 treatment prevented contraction of collagen gel induced by TGFβ (Figure 10C) over 48 hours but did not prevent basal level of contraction that was also observed with vehicle treated cells.

Since GKT137831 is a Nox1/4 dual inhibitor, we assessed the specific role of Nox4 by siRNA mediated Nox4 depletion. Knockdown of Nox4 decreased TGFβ induced αSMA+ myofibroblast differentiation by greater than 50% compared to control siRNA treated cells (Figure 10D). Quantitative reverse transcriptase-polymerase chain reaction (qRT-PCR) analysis demonstrated that we were able to deplete Nox4 mRNA by greater 80% and that Nox4 induction was significantly reduced in the presence of TGFβ (Figure 10E). Similar to GKT137831 experiments, Nox4 depletion did not affect TGFβ induced changes in myofibroblast genes SM22α or fibronectin but did inhibit the induction of Col1α1. To verify that Nox4 siRNA treatment was decreasing Nox4 generated cellular ROS, we assessed ROS changes by measuring fluorescence emission of a ROS sensitive

dye- dichlorofluorescein (DCF). TGFβ weakly induced DCF fluorescence above baseline levels and Nox4 depletion completely blunted the TGFβ mediated effect (Figure 10F). Furthermore, Nox4 knockdown did not affect basal DCF fluorescence. This suggests that most of the ROS generated by TGFβ, but not at the basal level, is through Nox4. As a positive control, 4.8 nM H_20_2 treatment also increased DCF fluorescence indicating viability of this assay to determine intracellular ROS changes (Figure 10F, bottom panel).

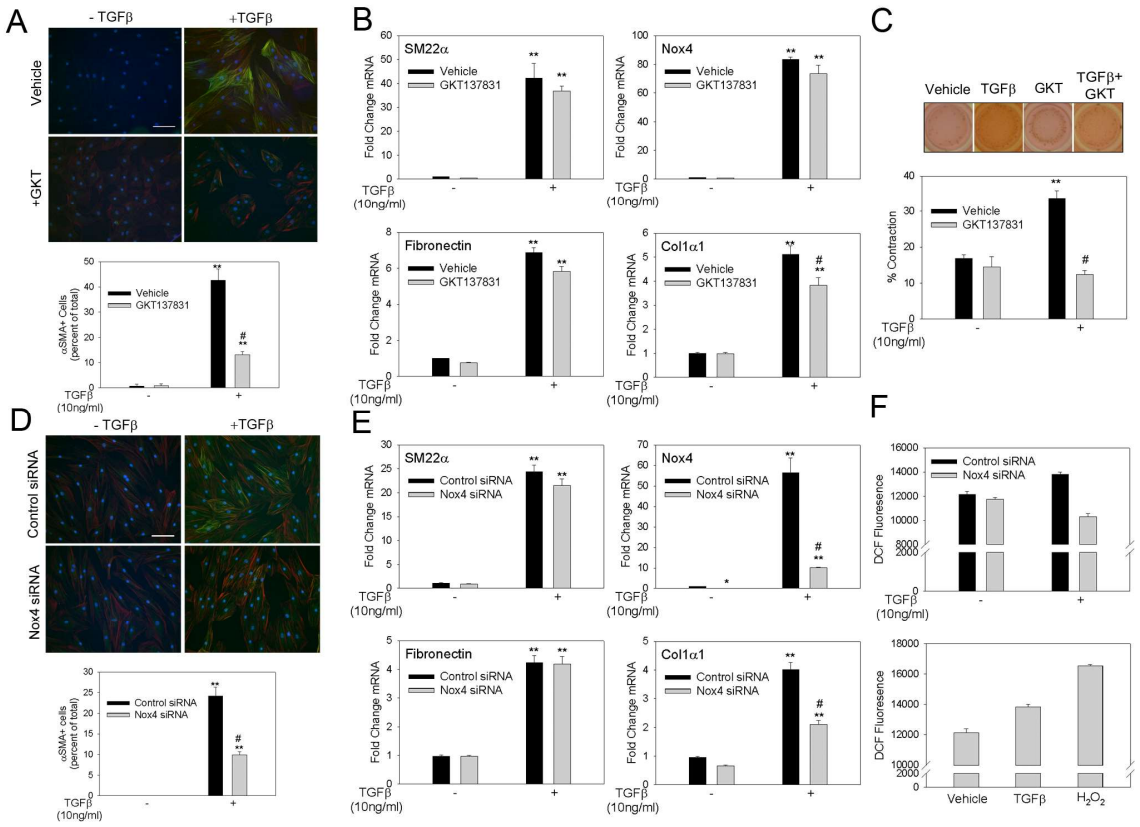

Figure 10: Nox4 inhibition with GKT137831 and Nox4 suppression with siRNA decreases dermal myofibroblast transformation.

A) Human dermal fibroblasts (hDF) were pre-treated with vehicle or GKT137831 (20 μM) for 1 h before stimulation with TGFβ for 48 h. Immunofluoresence staining for αSMA (green) and filamentous actin stain with phalloidin (red) was performed. The percent of αSMA+ myofibroblasts were quantified and averaged over the three experiments. B) hDF cells were pre-treated with vehicle or GKT137831 (20 μM) for 1 h followed by TGFβ (10 ng/ml) for 24 h. Cellular mRNA was analyzed via qRT-PCR for changes in gene expression of SM22α, Nox4, fibronectin and Col1α1. C) Collagen gel contraction assay was performed with hDF cells. Cells were treated with vehicle or GKT137831 (20 μM) in the presence or absence of TGFβ (10 ng/ml). Experimental groups were evaluated in triplicates. Change in gel surface area was determined after 48 h and is represented as the percent contraction of the gel. Data is presented as mean ± SEM. **P<0.05 vs. –TGFβ; #P<0.05 vs. vehicle + TGFβ treatment. D) hDF cells were electroporated with control or Nox4 siRNA and after 3 d were stimulated with TGFβ for 48 h. Immunofluoresence staining for αSMA (green) and phalloidin staining for filamentous actin (red) was performed to detect myofibroblasts. The percent of cells that transdifferentiate to myofibroblasts was determined. E) After electroporation of control or Nox4 siRNA, hDF cells were stimulated with TGFβ (10 ng/ml) for 24h and mRNA was collected to analyze changes in gene expression. F) To detect changes in reactive oxygen species (ROS), DCF-DA assay was performed on cells electroporated with control or Nox4 siRNA and incubated with or without TGFβ (10ng/ml). As a positive control, hDF cells electorporated with control siRNA were treated with 4.8 nM H_20_2. ROS detection assay was performed twice and each treatment group was evaluated in quadruplicates. All data is presented as mean ± SEM. **P<0.05 vs. –TGFβ; #P< 0.05 vs. control siRNA + TGFβ.

RelA is Dispensable For Nox4 Expression and Myofibroblast Transdifferentiation

It has been demonstrated that TNFα stimulation of human aortic SMCs leads to upregulation of Nox4 via activation of RelA- signaling (42). Furthermore, our lab has demonstrated that RelA is vital for lung epithelial cells to undergo TGFβ induced EMT and transdifferentiate into a myofibroblast-like cells (43). These lines of evidence led us to hypothesize that RelA may be involved in fibroblast to myofibroblast transdifferentiation via regulation of Nox4. First, we checked if TGFβ induced activation of RelA by inducing the phosphorylation of Ser536 or Ser276 on RelA TAD. Contrary to our hypothesis, TGFβ failed to induce phospho-Ser536-RelA (Figure 11A) or phospho-Ser276-RelA (data not shown). Furthermore, TGFβ did not induce degradation of IkBα. In contrast, TNFα, which served as a positive control, was a potent inducer of phospho-Ser536-RelA and of IkBα degradation. Since there was still a possibility that RelA was being activated via a different mechanism, we induced RelA knockdown using siRNA before stimulating hDF cells with

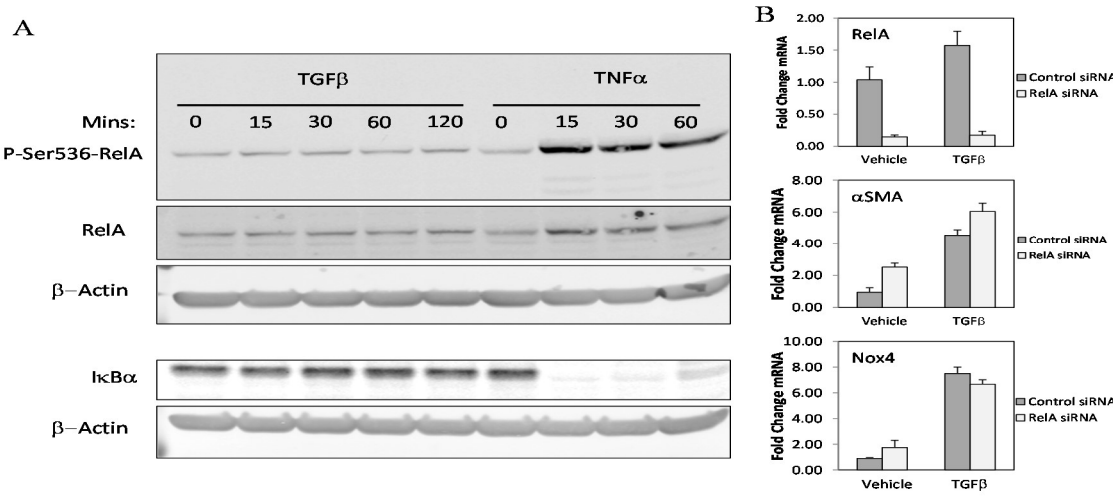

Figure 11: TGFβ does not induce RelA activation in human dermal fibroblasts.

A) hDF cells were stimulated with TGFβ or TNFα over 120 minutes before cell lysates were collected for Western blot analysis. B) hDF cells were electroporated with control or RelA siRNA and stimulated with TGFβ for 48 hours. Cell lysates were collected for gene expression analysis via qRT-PCR. Data is presented as mean ± SEM.

TGFβ. QRT-PCR analysis demonstrated that we achieved at least an 80% decrease in RelA mRNA abundance. Regardless, RelA depletion failed to inhibit αSMA, the key myofibroblast gene, and Nox4 (Figure 11B). We interpreted this data to mean that RelA signaling is not important in TGFβ mediated Nox4 upregulation or myofibroblast transdifferentiation.

SMAD3 REGULATES NOX4 AND MYOFIBROBLAST TRANSFORMATION.

After determining that Nox4 is an important mediator of hDF transdifferentiation to myofibroblast, we wanted to verify that Smad3 was the essential transcription factor involved in Nox4 gene expression and in myofibroblast transdifferentiation. Therefore, hDF cells were electroporated with control or Smad3 siRNA before TGFβ stimulation. Smad3 depletion with siRNA decreased αSMA+ myofibroblast formation by greater than 75% (Figure 12A) compared to control siRNA treated cells. In addition, TGFβ induction of SM22α in Smad3 depleted cells was blocked to a similar extent whereas expression of Nox4, fibronectin and Col1α1 was reduced by 25-30% of the level observed in control siRNA treated cells (Figure 12B). Western blot and qRT-PCR analysis suggested that we were able to deplete Smad3 with siRNA by 70-80% compared to control cells (Figure 12C). Interestingly, TGFβ also induced a decrease greater than 80% of Smad3 mRNA within 24h, suggesting that downregulation of Smad3 may be a negative feed-back loop to limit canonical Smad signaling.

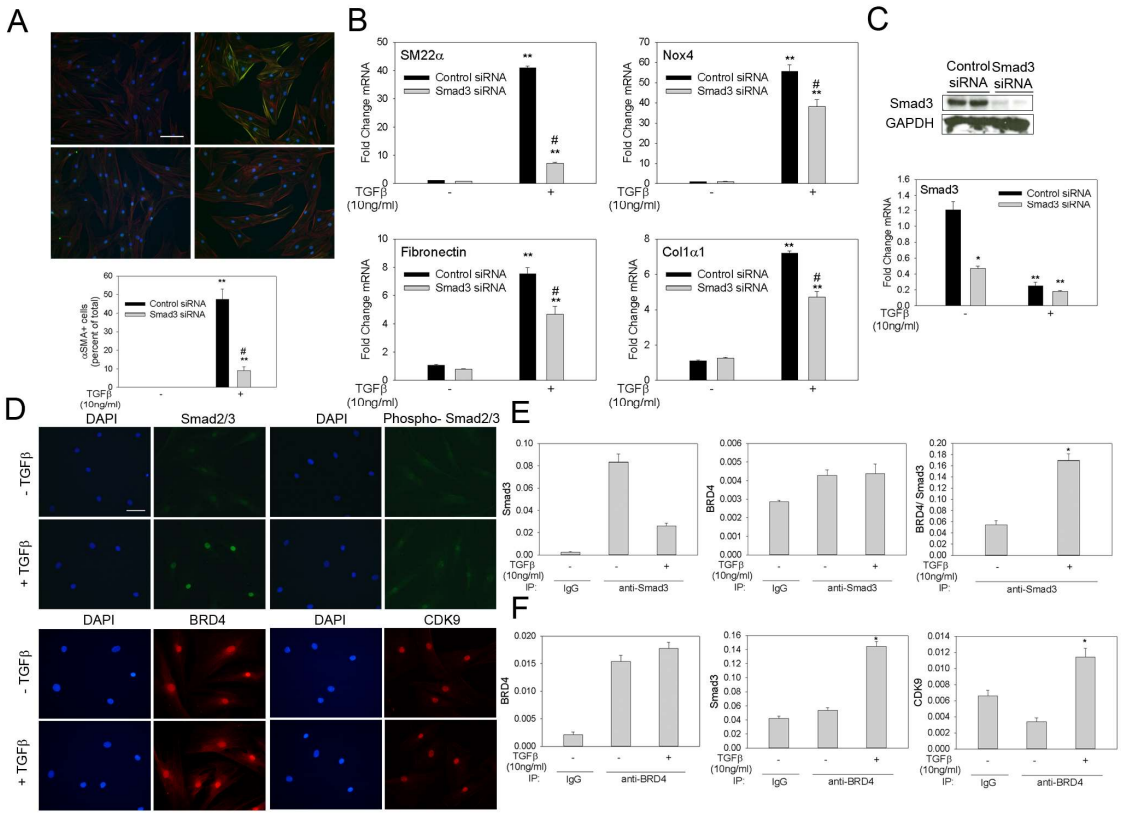

Figure 12: Smad3 regulates myofibroblast transdifferentiation and binds to BRD4 during TGFβ stimulation.

A) Human dermal fibroblasts (hDF) were electroporated with control or Smad3 siRNA. After 72 h incubation, cells were stimulated with TGFβ (10 ng/ml) for 48 h before immunostaining for αSMA (green) and phalloidin staining for filamentous actin (red). Data presented is the mean of three experiments. B) hDF cells were electroporated with control or Smad3 siRNA before being incubated with or without TGFβ (10 ng/ml) for 24 h. Changes in myofibroblast gene expression were determined via qRT-PCR. C) Whole cell extracts from hDF cells electroporated with control or Smad3 siRNA were collected 72 h after siRNA treatment and analyzed for their Smad3 content with Western blot. GAPDH was used as a loading control. Cells that were incubated with or without TGFβ (in B) were also evaluated for their level of Smad3 mRNA Data in A, B and C is presented as mean ± SEM. **P<0.05 vs. –TGFβ; #P<0.05 vs. vehicle + TGFβ . D) Immunofluorescence staining for Smad2/3, phospho-Smad2/3, BRD4 and CDK9 in hDF cells incubated with or without TGFβ (10 ng/ml) for 24 h. DAPI was used to stain nuclei. Scale bar represents 100 microns. E**)** hDF cells were treated with TGFβ (10 ng/ml) for 24 h. Equal amount of cell lysates were immunoprecipitated with anti-Smad3 antibody and subjected to SID-SRM-MS analysis of Smad3 and BRD4 protein levels. Data is presented as mean ratio of native to SIS peptides or as BRD4 signal normalized to Smad3. F**)** hDF cells were treated with TGFβ (10 ng/ml) for 24 h and cell lysates were immunoprecipitated with an anti-BRD4 antibody before being subjected to SID-SRM-MS analysis for BRD4, Smad3 and CDK9 proteins. Data is presented as a mean ratio of native to SIS peptide. Bar graphs represent mean ± SEM. *P<

SMAD3 DIRECTLY INTERACTS WITH THE TRANSCRIPTIONAL CO-ACTIVATOR BRD4.

We were able to verify that Smad3 plays a significant role in expression of Nox4 and other myofibroblast genes during myofibroblast differentiation. Next, we hypothesized that Smad3 may require transcription co-activators BRD4 and CDK9 to activate the fibrotic gene program since these proteins have been demonstrated, by our group and others, to be important in expression of inflammatory genes (44-46). Inflammation usually precedes fibrotic changes especially in skin, cardiac and lung pathologies and therefore involvement of these co-activators may be a common thread between two stages of healing. First, we wanted to determine whether Smad2/3 localizes with BRD4 and CDK9. Immunofluorescence staining for total Smad2/3 suggested that it accumulates within the nucleus after TGFβ stimulation (Figure 12D). To determine whether nuclear Smad2/3 was activated, we checked for the phosphorylated form of Smad2/3 and found it to be present only in the nuclei after exposure to TGFβ. In contrast, we observed BRD4 signal to be present predominantly in the nuclei with or without TGFβ treatment. Similarly, CDK9 signal was only observed in the nuclei suggesting that its primary involvement may be in transcription regulation. Next, we assessed whether Smad3 directly interacts with BRD4 and CDK9. Whole-cell extracts were enriched for Smad3 by immunoprecipitation followed by quantitative measurement of BRD4 and CDK9 via selected reaction monitoring-mass spectrometry (SID-SRM-MS). TGFβ treatment did not seem to increase Smad3 bound BRD4 (Figure 12E, middle panel). Assessment of total Smad3 indicated that TGFβ treatment leads to immunoprecipitation of significantly less amount of Smad3- ~25% of the amount enriched from control cells (Figure 12E, left panel). This aligns with our observation that TGFβ reduces Smad3 mRNA by 80% within 24h. Therefore, we normalized BRD4 signal to Smad3 to determine the fraction of BRD4 that was Smad3 bound. We found that normalized BRD4 signal increased by more than 3-fold after TGFβ

treatment (Figure 12E, right panel). In contrast, we did not observe any difference in CDK9 levels when comparing samples immunoprecipitated with normal IgG with samples immunoprecipitated with anti-Smad3 antibody, suggesting that Smad3 may not directly interact with CDK9 (data not shown). To verify that TGFβ induces the interaction of BRD4 with Smad3, we immunoprecipitated whole-cell extracts with anti-BRD4 antibody and measured bound Smad3. The enrichment of BRD4 was similar in control and TGFβ treated samples (Figure 12F, left panel). Furthermore, TGFβ treatment increased amount of Smad3 bound to BRD4 by approximately 3-fold (Figure 12F, middle panel), and increased CDK9 bound to BRD4 by approximately 4-fold (Figure 12F, right panel). Collectively, these data suggest that TGFβ increases Smad3 interaction with BRD4 and also increases BRD4 interaction with CDK9.

INHIBITION OF BRD4 WITH JQ1 OR BRD4 DEPLETION PREVENTS MYOFIBROBLAST TRANSDIFFERENTIATION.

Since BRD4 co-localizes with and is increasingly bound to Smad3 after TGFβ treatment, we asked whether BRD4 was necessary for Nox4 transcription and myofibroblast differentiation. JQ1, a small molecule inhibitor of BET domain containing proteins that competes for the bromodomain pocket used to bind to acetylated residues, was utilized as a BRD4 inhibitor. TGFβ treatment induced greater than 40% of hDF cells to transform to myofibroblasts and this transformation was completely blocked by JQ1 co-treatment (Figure 13A). Furthermore, 0.5 μM and 1 μM JQ1 treatment blocked not only TGFβ induced increases in SM22α, Nox4, fibronectin and Col1α1 mRNA but also decreased basal expression of SM22α, Nox4 and Col1α1 suggesting an important role of BET family of proteins in myofibroblast differentiation. The suppression of myofibroblast gene expression was almost the same with 0.5 μM and 1 μM JQ1 signifying high potency of this inhibitor even at low concentrations (Figure 13B). Importantly, JQ1 did not cause any cell death at either concentration. JQ1 also blocked TGFβ induced collagen gel

contraction without significantly affecting contraction that occurred at baseline in absence of TGFβ (Figure 13C).

To determine whether BRD4 is the main BET domain containing protein involved in myofibroblast transdifferentiation, BRD4 levels were depleted with siRNA in hDF cells. BRD4 knockdown blocked αSMA+ myofibroblast differentiation during TGFβ treatment (Figure 13D), which suggests that BRD4 is the essential BET domain containing protein responsible for de-novo synthesis of αSMA fibers. Gene expression analysis indicated that BRD4 depletion also diminishes TGFβ induction of SM22α and Nox4 by more than 50% compared to control siRNA treated cells (Figure 13E). Surprisingly, TGFβ induced transcription of fibronectin and Col1α1 was not affected by BRD4 knockdown. We interpret this to mean that another BET family member, in addition to BRD4, is involved in regulating myofibroblast genes. Lastly, Western blot and qRT-PCR analysis confirmed that we achieved at least an 80% reduction in BRD4 expression with siRNA treatment (Figure 13F).

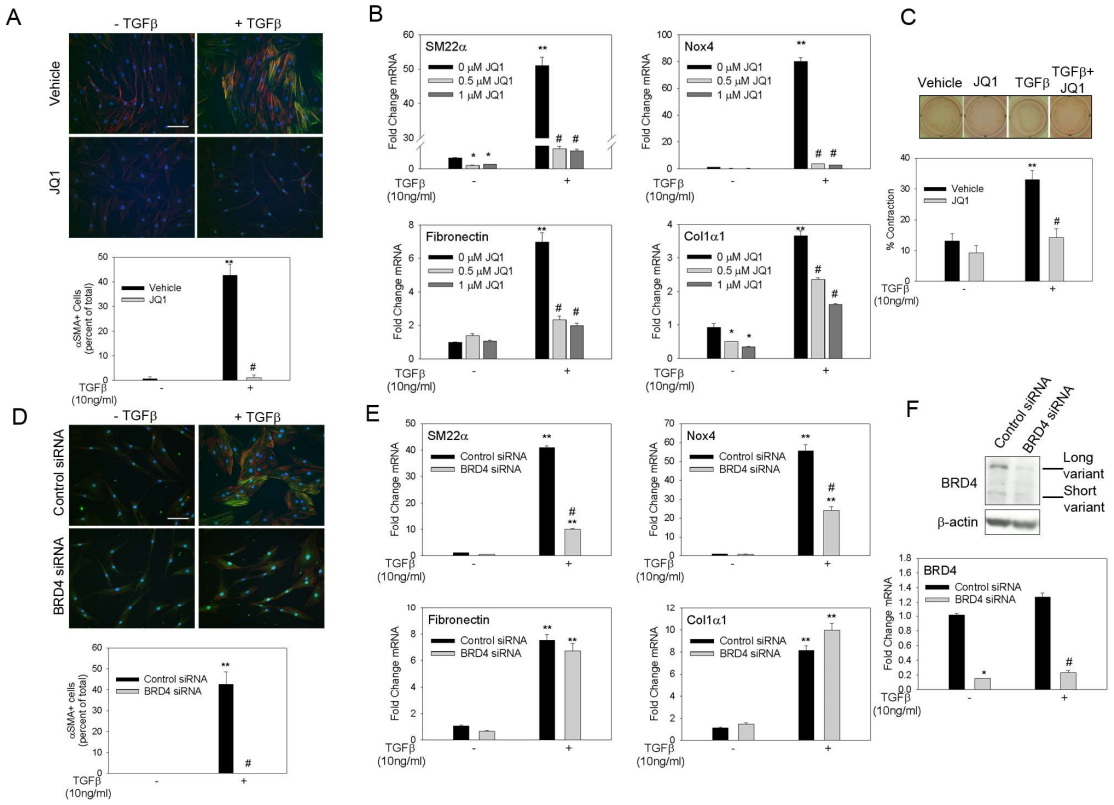

Figure 13: JQ1 treatment and BRD4 suppression with siRNA blocks myofibroblast transdifferentiation.

A) human dermal fibroblasts (hDF) cells were pre-incubated with 1 μM JQ1 or vehicle for 1 h before stimulation with TGFβ (10 ng/ml) for 48 h. Immunofluorescence staining for αSMA (green) and phalloidin staining for filamentous actin (red) was used to detect myofibroblasts. B) hDF cells were pre-incubated with 0.5 or 1 μM JQ1 for 1 h and then stimulated with TGFβ (10 ng/ml) for 24 h. mRNA was analyzed via qRT-PCR to determine myofibroblast gene expression changes. C) Collagen gel contraction assay was performed with hDF cells treated with vehicle or 1 μM JQ1 in the presence or absence of TGFβ (10 ng/ml). Gel surface area was measured at time 0 and 48 h and change in surface area is reported as percent contraction of gel. Data is reported as mean ± SEM. *P< 0.05 vs. 0 μM JQ1 – TGFβ; **P<0.05 vs. –TGFβ; #P<0.05 vs. vehicle + TGFβ. D) hDF cells were electroporated with control or BRD4 siRNA. After 72 h, cells were incubated with or without TGFβ (10 ng/ml) for another 48 h. αSMA immunostaining (green) and phalloidin staining for filamentous actin (red) was performed to quantify myofibroblasts (αSMA+ cells). E) hDF cells treated with control or BRD4 siRNA were incubated with or without TGFβ (10 ng/ml) for 24 h before being subjected to qRT-PCR analysis for myofibroblast genes. F) Knockdown efficiency of BRD4 was determined via Western blot and qRT-PCR. hDF cells were electroporated with control or BRD4 siRNA and whole-cell extracts were subjected to Western blot analysis. β-actin was used as a loading control. mRNA isolated from experiments in E was also used to assess the expression level of BRD4. Data is presented as mean ± SEM. *P< 0.05 vs. control siRNA – TGFβ; **P<0.05 vs. –TGFβ; #P<0.05 vs. control siRNA + TGFβ.

INHIBITION OF CDK9 WITH CAN508 OR CDK9 DEPLETION DIMINISHES MYOFIBROBLAST TRANSDIFFERENTIATION

During an inflammatory insult, transcription of full-length mRNA transcripts requires release of Pol II from its pause site which is mediated by phosphorylation of Pol II by CDK9- a component of P-TEFb. We hypothesized that CDK9 may also be necessary for transcription of fibrotic genes associated with myofibroblast differentiation. To test this hypothesis, a CDK9- specific small molecule inhibitor- Can508- was employed. Can508 successfully reduced TGFβ mediated αSMA+ myofibroblast transformation by 80% relative to vehicle treated cells (Figure 14A). In addition, Can508 inhibited Nox4 mRNA transcription by more than 90% at baseline but had less effect on Nox4 mRNA during TGFβ stimulation (~15% reduction compared to vehicle treated cells, Figure 14B). In contrast, Can508 was a very potent inhibitor of SM22α, fibronectin and Col1α1 mRNA both at baseline and during incubation with TGFβ, reducing gene expression by 40-90% compared to vehicle treated cells (Figure 14B). To determine the effect of CDK9 inhibition on myofibroblast contractility, Can508 was embedded in collagen gels in the presence or absence of TGFβ. Can508 treatment reduced collagen gel contraction under basal conditions (in absence of TGFβ) and also significantly reduced contraction during TGFβ stimulation (Figure 14C). Taken together with immunofluorescence data, this suggests that blockade of CDK9 activity decreases stress fiber formation and thereby hinders the generation of contractile force.

Since Can508 may have off-target effects, we depleted CDK9 with siRNA in hDF cells to verify its role in myofibroblast differentiation. CDK9 depletion inhibited TGFβ induced αSMA+ myofibroblasts transformation by approximately 50% as assessed by immunofluorescence microscopy (Figure 14D). Furthermore, CDK9 knockdown diminished TGFβ induction of Nox4, SM22a, fibronectin and Col1a1 by approximately 25-90% relative to the level observed in control cells (Figure 14E). This demonstrated to us that CDK9 plays a vital role in the transdifferentiation process by regulating

myofibroblast gene transcription. Western blot analysis confirmed that CDK9 siRNA treatment decreases CDK9 protein levels by more than 80% compared to control siRNA treated cells (Figure 14F). In addition, CDK9 mRNA was suppressed to a similar extent with CDK9 siRNA treatment (Figure 14F).

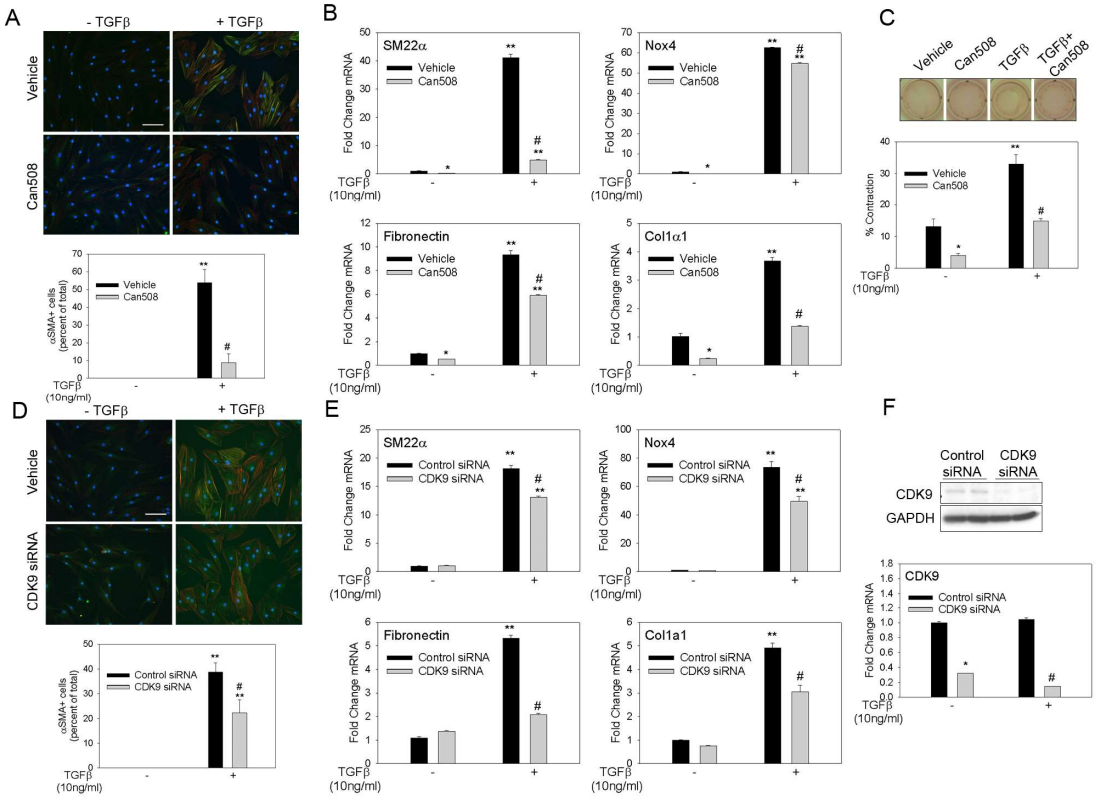

Figure 14: Inhibition of CDK9 with Can508 or CDK9 knockdown with siRNA decreases myofibroblast transformation.

A) human dermal fibroblasts (hDF) were pre-treated with Can508 (30 μM) for 6 h before stimulation with TGFβ (10 ng/ml) for 48 h. Immunofluorescence for αSMA (green) and phalloidin staining for f-actin (red) was performed. αSMA+ myofibroblast cells were quantified. B) Myofibroblast gene expression changes were analyzed via qRT-PCR in hDF cells pre-treated with Can508 and stimulated with TGFβ (10 ng/ml) for 24 h. C) Collagen contraction assay was performed on hDF cells treated with vehicle or Can508 (30 μM) in the presence or absence of TGFβ (10 ng/ml). Change in surface area is reported as percent contraction of the gels. Data is represented as mean ± SEM. *P< 0.05 vs. vehicle – TGFβ; **P<0.05 vs. –TGFβ; #P<0.05 vs. vehicle + TGFβ. D) hDF cells were electroporated with control or CDK9 siRNA before being stimulated with TGFβ (10 ng/ml) for 48 h. Cells were immunostained for αSMA and also stained for f-actin with phalloidin (red) to determine the myofibroblast population. E) hDF cells were subjected to qRT-PCR analysis for myofibroblast gene expression changes after electroporation of control or CDK9 siRNA and incubation with or without TGFβ (10 ng/ml) for 24h. F) CDK9 knockdown was verified via Western blot and qRT-PCR analysis. hDF cells were electroporated with control or CDK9 siRNA. After 72h, whole-cell extracts were used for running of SDS-PAGE and Western blot. GAPDH was use as a loading control. mRNA isolated in E was also used for qRT-PCR analysis of CDK9 gene expression. Data is presented as mean ± SEM of at least three experiments. *P< 0.05 vs. control siRNA – TGFβ; **P<0.05 vs. –TGFβ; #P<0.05 vs. control siRNA + TGFβ.

TGFβ INDUCES THE RECRUITMENT OF P-SMAD3, BRD4 AND CDK9 ON THE NOX4 PROMOTER.

Since TGFβ induced transcription of Nox4 requires transcription regulatory proteins including Smad3, BRD4 and CDK9, we inferred that they must accumulate near the Nox4 transcription start site (TSS). Using dual cross-link chromatin immunoprecipitation (X-ChIP) assay we assessed for the enrichment of these proteins on the Nox4 gene (Figure 15). TGFβ treatment of hDF cells for 24h led to a 4.3-fold enrichment of P-Smad3, the activated form of the transcription factor, while this enrichment was blocked by presence of 1 μM JQ1. In addition, BRD4 was enriched by a striking 12.2-fold in presence of TGFβ and JQ1 reduced BRD4 accumulation to 1.9-fold compare to control. Similarly, TGFβ also induced a 6.4 –fold enrichment of CDK9 relative to control which was also blocked by JQ1. BRD4 and CDK9 are both capable of phosphorylating Pol II at Ser2 to promote transcription elongation. Therefore we assessed for P-Ser2-Pol II enrichment near Nox4 TSS. TGFβ induced a 2.6-fold enrichment of P-Ser2-Pol II on the Nox4 gene and JQ1 treatment blocked this enrichment. These data indicate that TGFβ induces the recruitment of Smad3-BRD4-CDK9 complex to the Nox4 gene which promotes P-Ser2-Pol II formation leading to transcription elongation of Nox4 mRNA transcripts- a key regulatory step in myofibroblast transdifferentiation.

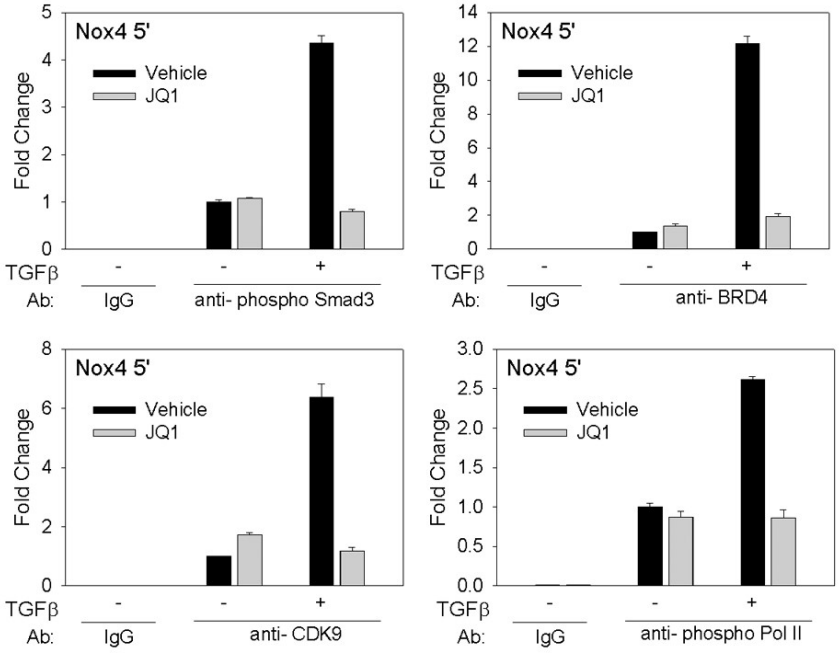

Figure 15: Increase accumulation of Smad3, BRD4 and CDK9 on Nox4 promoter after TGFβ stimulation.

Human dermal fibroblasts were pre-incubated with vehicle or JQ1 for 1 h before being stimulated with TGFβ (10 ng/ml) for 24 h. Cells were then subjected to XChIP analysis of Smad3, BRD4, CDK9 and phospho-Ser2- Pol II on the Nox4 promoter. Chromatin immunoprecipitated with a non-specific IgG was used as negative control. Fold change was determined compared to –TGFβ sample. Data is presented as mean ± SEM. XChIP experiment was repeated twice and similar results were obtained.

INCREASED SENSITIVITY OF HTS FIBROBLAST TO TGFβ IS BLOCKED BY JQ1

We have previously demonstrated that HTS fibroblasts are hyper-sensitive to IL-6 transsignaling and express higher levels of ECM genes and cell proliferation markers which can be abrogated by interfering with signal transducer and activator of transcription-3 (STAT3) (47). Therefore, we investigated whether HTS fibroblasts also display an exaggerated response to TGFβ and whether this phenotypic behavior can be modified with

JQ1- an inhibitor that demonstrated a potent ability to block transcription of Nox4 and other myofibroblast genes. Immunofluorescence analysis for αSMA demonstrated that there were relatively more HTS myofibroblasts than NBS myofibroblasts under basal conditions and treatment with JQ1 reverted most of the myofibroblast population back to its quiescent state (Figure 16A). Incubation with TGFβ increased myofibroblast population 4- to 5-fold in both cell types but co-treatment with JQ1 not only blocked the induction of αSMA-positivity but also decreased the myofibroblast population to levels observed with JQ1 treatment alone. Since JQ1 was very potent at decreasing αSMA stress fibers, we next evaluated its ability to modify myofibroblast gene transcription. QRT-PCR analysis for myofibroblast genes indicated that Nox4, fibronectin and Col1α1 mRNA levels were significantly elevated (2.5 to 3-fold) at baseline in HTS fibroblasts compared to NBS fibroblasts while increase in SM22α mRNA did not reach statistical significance (Figure 16B). Furthermore, TGFβ induced elevation in mRNA of all four genes but HTS fibroblast displayed an even higher induction (by ~2-fold) of ECM genes fibronectin and Col1α1. JQ1 co-treatment at 0.5 μM and 1 μM blocked TGFβ induction of myofibroblast genes or even suppressed them below baseline levels. Since we identified SM22α and Nox4 gene transcription to be BRD4-dependant in earlier experiments, we asked whether BRD4 also controlled their transcription in HTS fibroblasts- a cell type which displays signs of an altered transcriptional program. BRD4 depletion with siRNA suppressed TGFβ induction of both SM22a and Nox4 by more than 50% suggesting that BRD4 regulates these gene in HTS fibroblasts as well (Figure 16C). Collectively, these data demonstrate that HTS harbor greater population of myofibroblast than NBS; that HTS fibroblasts have elevated expression of myofibroblast genes in the presence and absence of TGFβ; and that these cells require BET family of protein, including BRD4, to maintain their transformed phenotype.

HTS Fibroblast Have Increase Accumulation of Smad3 and BRD4 on Nox4 Promoter

Nox4 is key to development of αSMA fibers and Col1α1 production and it is a gene that is highly elevated under basal conditions in HTS fibroblasts. Therefore we examined whether elevated expression of Nox4 was due to increase loading of transcription factor Smad3 and co-regulator BRD4 on the Nox4 gene. X-ChIP analysis demonstrated that there was increased accumulation of Smad3 (by ~3-fold) in HTS cells on the Nox4 5' end (Figure 16D). Furthermore, TGFβ induced enrichment of Smad3 on the Nox4 gene by 2.7-fold in NBS cells and by 5.2-fold in HTS cells. Similarly, there was more accumulation of BRD4 on the Nox4 gene in HTS cells- a 2.3-fold increase compare to NBS cells. TGFβ also induced accumulation of BRD4 on the Nox4 gene by 2.8-fold in NBS fibroblast and by 5.8-fold in HTS fibroblasts. Together with qRT-PCR data, these data suggest that elevated expression of myofibroblast genes in HTS fibroblast may be due to increase in basal accumulation of Smad3 and BRD4 that leads to enhanced transcription.

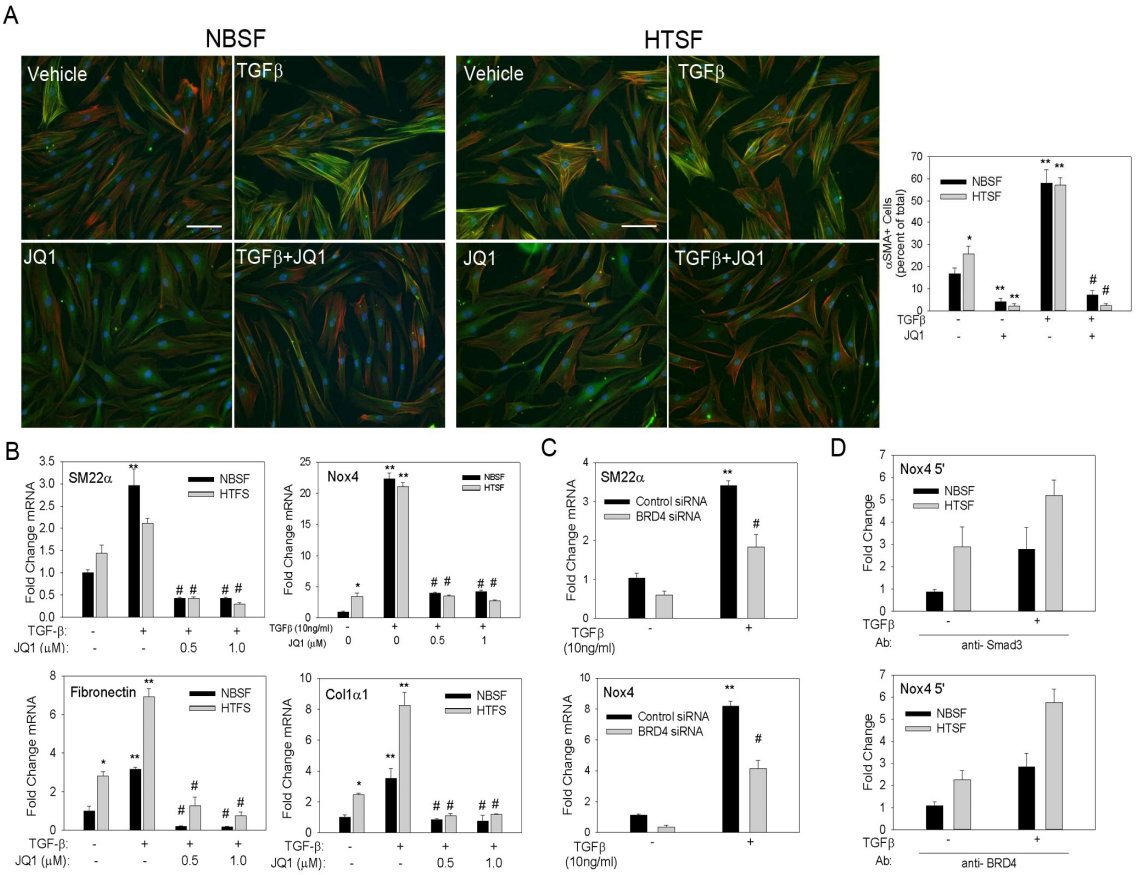

Figure 16: Hypertrophic scar fibroblasts have increase propensity for myofibroblast transformation, which can be blocked with JQ1.

A) Hypertrophic scar (HTS) and non-burn skin (NBS) fibroblasts were pre-incubated with vehicle or JQ1 (1 μM) for 1 h before being stimulated with TGFβ (10 ng/ml) for 48 h. Cells were then immunostained for αSMA (green) and co-stained for f-actin with phalloidin (red). Data is presented as mean ± SEM. *P= 0.055 vs. NBSF; **P<0.05 vs. unstimulated cells; #P<0.05 vs. TGFβ. B) NBS and HTS fibroblasts were subjected to qRT-PCR analysis of myofibroblast gene expression changes after incubation with or without JQ1 (1 μM) and TGFβ (10 ng/ml). Data is presented as mean ± SEM. *P< 0.05 vs. NBSF; **P<0.05 vs. unstimulated cells; #P<0.05 vs. TGFβ. C) BRD4 knockdown with siRNA was performed in HTS fibroblasts before TGFβ (10 ng/ml) stimulation for 24 h. Cellular mRNA was extracted and qRT-PCR was performed for BRD4-dependant myofibroblast genes. **P<0.05 vs. control siRNA –TGFβ; #P<0.05 vs. control siRNA + TGFβ. D) XChIP analysis for Smad3 and BRD4 on the Nox4 promoter was performed on NBS and HTS fibroblasts incubated with or without TGFβ (10 ng/ml) for 6 h. Fold change is calculated relative to NBSF – TGFβ sample. XChIP experiment was performed twice and similar results were observed. Data is presented as mean ± SEM.

SUMMARY AND DISCUSSION

HTS is a devastating sequelae of burn injury that is characterized by excess deposition of ECM and by overabundance of αSMA+ myofibroblasts. In cardiac and lung fibroblasts, ROS generated by Nox4 is vital for fibroblast to myofibroblast transformation and for synthesis of ECM proteins. The role of Nox4 in dermal fibroblast has not been elucidated to date. In addition, the role of transcriptional co-activators such as BRD4 and CDK9 in the transcription regulation of Nox4 and myofibroblast genes has not been described. In this study, we verified that myofibroblasts are present in HTS soon after burn injury and are also a major source of TGFβ- the potent cytokine responsible for myofibroblast transformation. Dermal fibroblasts develop αSMA+ stress fibers, highly upregulate Nox4 and SM22α and increase transcription of ECM genes fibronectin and Col1α1 after exposure to TGFβ. We demonstrate using a small molecule inhibitor GKT137831 and Nox4 knockdown that Nox4 is involved in αSMA fiber formation and collagen transcription in hDF cells. Nox4 transcription is controlled by Smad3 during TGFβ stimulation but also requires the epigenetic reader and transcription co-activator BRD4. BRD4 interacts with Smad3 and with CDK9, part of P-TEFb complex which is necessary for Pol II phosphorylation on Ser2 to induce full length transcripts of Nox4. We found that HTS fibroblast express high levels of myofibroblast genes, including Nox4, under basal conditions and have a more robust response to TGFβ than NBS fibroblasts, which can be inhibited by JQ1- a small molecule inhibitor of BRD4 and BET family of proteins. Mechanistically, HTS fibroblasts have more loading of Smad3 and BRD4 on the Nox4 promoter even in absence of TGFβ suggesting that overactivation of the canonical Smad pathway may be the reason for the hyperresponsive cellular phenotype.

Interestingly, we found that inhibition of Nox4 activity with GKT13831 or its suppression with siRNA had limited effect on myofibroblast genes in hDF cells. Nox4 was necessary for induction of αSMA and collagen but dispensable for SM22α and fibronectin.

Previous work using fetal and adult lung fibroblast (31) and cardiac fibroblast (48) suggested a role of Nox4 generated ROS in regulation of fibronectin. The discrepancy may be due to the different origins of the fibroblast that were studied. Indeed, global gene expression analysis of human fibroblasts from 43 different anatomic sites suggests systematic differences in gene expression with respect to anterior-posterior, proximal-distal and dermal-nondermal origin (1) and therefore suggests differences in gene regulation. In dermal fibroblasts from systemic sclerosis patients, Nox4 was highly expressed (49), similar to our observation in HTS fibroblasts, and was upstream of Col1 expression. Surprisingly, Nox4-deficiency in mice delayed wound closure but did not affect presence of αSMA+ myofibroblasts over a two week period suggesting that αSMA induction is not entirely dependent on Nox4 in vivo (50).

Investigation of transcription factor binding regions that control Nox4 expression have identified a 4 kb Smad binding element (SBE) upstream of TSS that is necessary for Smad3 binding and transcription of Nox4. Recent work using Nox4 promoter constructs in mouse embryonic fibroblast (MEF) cell line identified a contributory role of a CArG box, the binding element of myocardin related transcription factor (MRTF), in regulating Nox4 expression (51). Authors also demonstrated that a SBE upstream of the CArG box was more important for Nox4 promoter activity in kidney epithelial cells, whereas the CArG box was essential in MEF cells. In addition, the Hippo pathway transcription factors TAZ/YAP were upregulated under low-calcium+ TGFβ treatment of kidney epithelia and their downregulation prevented Nox4 expression. Sp3 is another transcription factor with affinity for GC-boxes on the Nox4 promoter. Downregulation of Sp3 decreased Nox4 promoter activity in a human epithelial cell line (52). Our work is congruent with these studies and demonstrates that downregulation of Smad3 decreases but does not abolish Nox4 expression. This suggests other transcription factors such as MRTF may also be involved in regulating Nox4 in hDF cells.

Since Smad3 is important in the transcription of Nox4 and other myofibroblast genes during myofibroblast transformation (Figure 12B), we asked what other transcription co-activators complex with Smad3 and are required for the transdifferentiation process. BRD4 is an important adaptor protein that couples the multimeric Mediator complex with transcription factors and promotes Pol II activation. It can phosphorylate Pol II directly or recruit P-TEFb (CyclinT1/CDK9) to Pol II via its C-terminal domain. The BD domain of BRD4 is known to interact with acetylated histones and acetylated transcription factors such as TWIST (involved in EMT) and RelA/NF-κB suggesting that acetylated histones and transcription factor serve as important signals for recruitment of transcription machinery. We demonstrate for the first time that BRD4 binds directly to Smad3 and BRD4 downregulation suppresses a subset of Smad3-dependant myofibroblast genes. In addition, BRD4 accumulates, along with Smad3 and CDK9, on Nox4 promoter during TGFβ treatment. There is evidence that p300/CBP acetylates Lys-372 and Lys-19 of Smad3 leading to enhanced Smad3 transcriptional activity. This suggests that one or both of the acetylated residues may serve as docking sites for BRD4, but more work is needed to verify the regions of Smad3-BRD4 interaction. Although JQ1 inhibited all myofibroblast gene expression, BRD4 suppression decreased αSMA fibers and Nox4 and SM22 mRNA, but mRNA of fibronectin and Col1α1 remained unaffected. We interpret this to mean that another BET protein such as BRD2 may also be involved in myofibroblast transformation. In lung fibroblasts, BRD2 depletion decreased TGFβ induced αSMA expression (46) which suggests that it may have a role in regulating other myofibroblast genes.

P-TEFb is a complex of CyclinT1 and CDK9 that phosphorylates Pol II on Ser2 to promote transcription elongation. CDK9 mediated activation of Pol II has been demonstrated to be important during viral infection and during activation of innate immunity (53). Here, we demonstrate that CDK9 is also important in expression of myofibroblast genes and specifically for Nox4 expression. TGFβ induced enrichment of CDK9 and promoted phosphorylation of Pol II Ser2 on the Nox4 promoter. Although we

were unable to detect CDK9 in Smad3 immunoprecipitates, we found that CDK9 suppression inhibited the expression of myofibroblast genes that were also Smad3-dependent. This suggests that Smad3 may not directly interact with CDK9 although CDK9 is part of the transcriptional machinery that regulates Smad3-dependant genes. BRD4 is an intermediate protein that binds to Smad3 and CDK9 and may be one key link between the transcription factor and Pol II activation apparatus.

We have previously demonstrated that HTS fibroblasts express higher levels of gp130- part of the IL-6 receptor complex- and exhibit an exaggerated response to IL-6 leading to higher expression of Col1α2 and fibronectin (47). Here, we demonstrate that HTS fibroblasts express significantly high levels of Nox4, fibronectin and Col1α1 under basal conditions and upregulate the expression even more with TGFβ compare to NBS fibroblasts. Our experiments with hDF cells suggested a role of Smad3-BRD4 complex in mediating Nox4 expression and myofibroblast transformation. Therefore we asked whether the enhanced expression of Nox4 was due to increase loading of Smad3 and BRD4 on the Nox4 promoter in HTS cells. Results from X-ChIP experiments validated our hypothesis and suggested that increased basal activation of the Smad pathway coupled with BRD4 on the Nox4 gene promoter drives the myofibroblast phenotype in HTS cells. This was supported by our qRT-PCR experiments which demonstrated that inhibition of BRD4 with JQ1 abolishes the myofibroblast phenotype in HTS cells during TGFβ stimulation. Similar to our observations in HTS cells, increased loading of BRD4 and acetylated-H4K5 chromatin mark on the IL-6 promoter was observed by Tang X and colleagues in lung fibroblasts from IPF patients (46). Recently, it has been reported that JQ1 administration before or after onset of hepatic fibrosis in a mouse model limits ECM deposition and decreases myofibroblast makers (44). Collectively, these finding support an important role of Smad signaling and BET proteins, including BRD4, in myofibroblast transdifferentiation and fibrosis.

In summary, we describe an important role of transcription co-activators BRD4 and CDK9 in regulation of Nox4 and other myofibroblast genes. Furthermore, we demonstrate that overactivation of the myofibroblast gene program in HTS can be blocked and reversed by JQ1. These findings suggest that inhibitors of BET family of proteins may be useful in limiting HTS after burn injury.

The expanded study was published in the journal *Cell Death & Disease* (54).

Appendix A: Materials and Methods for Ang II *In Vivo* Experiments

Animal care and use

C57Bl/6 mice (stock# 000664) and mT/mG Cre-reporter mice on C57Bl/6 background (stock# 007676) were purchased from The Jackson Laboratory (Bar Harbor, ME). Col1α2-CreER^T mice (backcrossed into C57Bl/6 background) were a gift from Dr. Arjun Deb (University of North Carolina, Chapel Hill). This transgenic mouse was originally created by Zheng B. and colleagues at University of Texas M.D. Anderson Cancer Center (23). RelA-flox (RelA f/f) mice containing loxP sites in intron-4 and -8 of the *RelA* gene were generated in our laboratory (55) and backcrossed 8 times into C57Bl/6 background. Briefly, a gene targeting vector containing loxP sites and a neomycin positive-selection cassette was electroporated into 129B6F1 mouse embryonic stem cells. After drug selection, cell colonies that survived were screened for homologous recombination at the *RelA* locus. Clones that had incorporated the loxP sequences were then injected into C57Bl/6 blastocysts. The resultant chimeras were crossed with FLPeR mice to remove the neomycin cassette from the mutant *RelA* allele. Two clones were generated, of which one was backcrossed with C57Bl/6 mice to segregate the FLP1 transgene and to establish the RelA-flox line. The RelA f/f mice developed normally, were fertile and expressed RelA at a level similar to wild-type mice.

To characterize the specificity of CreER^T recombinase activity in Col1α2-CreER^T mice, mT/mG mice were mated with a Col1α2-CreER^T transgenic. The resultant progeny, mT/mG•Col1α2-CreER^T- and mT/mG•Col1α2-CreER^T+, was administered 1 mg tamoxifen per day for 10 consecutive days. Tissues were isolated two weeks after the last injection for identification of cells that underwent Cre-mediated recombination.

For hypothesis testing, RelA f/f mice were mated with Col1α2-CreER^T mice to generate RelA f/f•Col1α2-CreER^T– and RelA f/f•Col1α2-CreER^T+ transgenic animals. Tamoxifen (1 mg/day) was administered to both genotypes via i.p. injections for 10 consecutive days. Mice harboring Col1α2-CreER^T were then classified as RelA conditional knockout (RelA-/-) while those without Col1α2-CreER^T were considered as RelA- wild-type (RelA+/+). RelA+/+ and RelA-/- mice were infused with saline (sham) or angiotensin II (Ang II) 3 weeks after the last tamoxifen injection or their aortas were isolated for characterization by flow cytometry and qRT-PCR.

Tamoxifen (Sigma) was dissolved in 10 % ethanol and 90 % corn oil to make a 10 mg/ml stock solution for administration via i.p. injections. Both male and female mice were utilized in the experiments. Mice were 3-4 weeks old at the start of tamoxifen treatment and 9-12 weeks old at the time the Ang II infusion experiments were performed.

Ang II was delivered at a rate of 2,500 ng/kg/min for 7 days via subcutaneous Alzet osmotic minipump (Durect Corporation) while saline-infused animals were used as controls. Ang II was synthesized by University of Texas Medical Branch (UTMB) Peptide Synthesis Core or purchased from Sigma. All animal experiments performed as part of this study were approved by the UTMB Institutional Animal Care and Use Committee.

Ultrasonography

Abdominal aortas of mice, from diaphragm to the renal arteries, were imaged using Vevo2100 ultrasound imaging system (VisualSonics, Toronto, Canada) at baseline and during Ang II infusion (day 6). Mice were sedated with 1 % isoflurane in a supine position during the imaging process. *In vivo* ultrasound imaging allowed us to determine changes in aortic dilation and to visualize dissections during Ang II infusion. Aortic diameter measurements were made in triplicate at the site of maximum dilation in the supra-renal aorta of each mouse.

Flow cytometry

At experiment termination, mice were euthanized in accordance with the animal use protocol and American Veterinary Medical Association guidelines, and whole aortas were isolated and periadventitial fat was removed under a dissecting scope. Aortas were then minced into small pieces and incubated in a digestion buffer containing 0.6 U/ml Liberase Blendzyme (Roche), 50 µg/ml Elastase (Sigma), and 0.1 % BSA in DMEM/F12 base media. Aortic tissue was digested for 1-1.5 hours at 37° C on a vertical rotator. After complete digestion, cells were filtered through a 100 µm cell strainer and washed with FACS buffer (0.5 % BSA and 0.02 % NaN3 in DMEM). RBCs were removed using a lysis buffer from Qiagen. All antibodies were purchased from eBioscience unless stated otherwise. The Fc receptors on leukocytes were blocked with anti-CD16/32 antibody. Fluorochrome-conjugated antibodies against surface antigens were then added, including anti-CD45 (30-F11), anti-CD31 (390), anti-PDGFRα (APA5), anti-CD90.2 (53-2.1), anti-NK1.1 (PK136), anti-CD49b (DX5), anti-CD45R (RA3-6B2), anti-Ly6G (1A8, BD Pharmigen), anti-CD11b (M1/70), anti-F4/80 (BM8), anti-Ly6C (HK1.4) and incubated for 30 minutes. Cells were washed twice, fixed and permeabilized (eBioscience solution) and then incubated with fluorochrome-conjugated antibodies against intracellular antigens including anti-αSMA (1A4, Sigma) and anti-RelA (D14E12, Cell Signaling) for 30 minutes. At the end of the incubation period, cells were washed again and lightly fixed in 0.5 % PFA solution before being analyzed with BD LSRFortessa cell analyzer. Data were evaluated using FlowJo software. Dead cells and debris, as defined by a high forward scatter, were excluded from analysis.

Immunohistochemistry (IHC)

After aortic perfusion with PBS to remove all circulating blood cells, supra-renal abdominal aortas were isolated, embedded in optimal cutting temperature (OCT) compound and sectioned (8 µm thickness) using a cryostat. Aortic cross-sections were blocked with 5 % goat serum before being incubated with primary antibodies overnight at

4° C. Antibodies utilized were rabbit anti-phospho-Ser536-RelA (Cell Signaling), rabbit anti-RelA (Santa Cruz), rabbit anti-IL6 (eBioscience), rat anti-MCP-1 (Abcam) rabbit anti-αSMA (Abcam) and rabbit anti-PDGFRα (eBioscience). AlexaFluor-568 conjugated goat anti-rabbit or AlexaFluor-488 conjugated goat anti-rat secondary antibodies (ThermoFisher Scientific) were utilized for detection via immunofluorescence. To detect phospho-Ser536-RelA, the signal was amplified via an avidin-biotin kit (PK6101, Vector labs) and visualized with DAB chromogen. Secondary antibody-only negative controls were used to determine specificity of the immunostaining. Images were obtained using DXM1200F Nikon Digital Camera attached to a Nikon Eclipse 80i microscope. LSM 510 Meta UV confocal microscope was used for analysis of αSMA and PDGFRα immunostaining.

Histological characterization

Formalin-fixed tissue sections of abdominal aortas were stained with Hematoxylin and Eosin using standard procedures to determine changes in cellular composition. Images were captured at 200x magnification and adventitial area was quantified using ImageJ software (NIH). The adventitia was defined as the area between external elastic lamina and tunica externa. The adventitial area from three different aortic cross-sections per mouse was analyzed and averaged, and n = 5-7 abdominal aortas were evaluated in each group.

Quantitative real-time PCR (qRT-PCR)

RNA was extracted from whole aortas using Trizol reagent (Sigma) and quantified with a Nanodrop apparatus (Thermo Scientific). Samples with 260/280 ratio >1.6 were used for further analysis. One μg RNA was reverse transcribed using Superscript III Reverse Transcriptase System (Invitrogen) and diluted 1:2 with DEPC-treated water. Real-time PCR reactions utilizing iQ SYBR Green Supermix (Bio-Rad) were run in triplicates in a CFX96 Real-Time Detection System (Bio-Rad). 18s rRNA was used as the internal

control. Primers used in the real-time reactions are listed in Supplementary Table 1. Relative mRNA abundance was calculated using the ΔΔCT method.

Blood pressure measurements

Blood pressure measurements were made as previously described (56). Briefly, arterial blood pressure and heart rate were recorded using a non-invasive tail-cuff method (Kent Scientific, Torrington, CT) on at least 4 consecutive days at baseline and during Ang II infusion. Mice were acclimated to the tail-cuff inflation for several days prior to osmotic minipump implantation. Measurements are reported as mean ± SEM.

Data analysis

Data are reported as mean ± SEM. Statistical analyses were performed using SigmaPlot 12.0 (SYSTAT software, San Jose, CA). Student's t-test was used to analyze differences between two groups. One-way RM ANOVA on Ranks was utilized to determine differences between multiple groups over time followed by Tukey's post-hoc test for group-wise comparison. Fisher's exact test was performed on AAA data set. $P < 0.05$ was considered to be significant.

Appendix B: Materials and Methods for Myofibroblast Transdifferentiation Experiments

Cell culture and tissue biopsies

Skin biopsies were acquired from pediatric burn patients (ages 0-18 years) at 12, 24 and 48 months following burn injuries covering approximately 20% of the body surface area as part of a study approved by IRB at the University of Texas Medical Branch. The biopsies were taken from the site of HTS or the adjacent NBS region during surgical revision procedure. Samples were formalin fixed, paraffin embedded and sectioned at 4 microns thickness. Fibroblasts from HTS and NBS biopsies were isolated as previously described (57) and propagated in DMEM containing 15% fetal bovine serum (FBS) and 1% anti-biotic/anti-mycotic (Invitrogen). Experiments were performed on NBS and HTS cells from equivalent passages. Cells from passage 6 through 15 were used in the experiments. For experiments involving TGFβ, NBS and HTS cells were serum starved overnight in media containing 0.5% FBS. Normal adult hDF were bought from Lonza and cultured in the manufacturer recommended media. All experiments with hDF cells were performed on cells from passage 4 through 12.

Reagents and antibodies

Human TGFβ1 (Peprotech, # 100-21) was suspended in vehicle containing BSA, as recommended by the manufacturer, at 10 μg/ml stock concentration. Aliquots were kept frozen at -20˚C until needed. GKT137831 was gift from Genkyotex., JQ1 and LY2157299 were purchased from Apexbio and Can508 was purchased from Santa Cruz.

The following primary antibodies were used for IHC or immunofluorescence: anti-TGFβ (Abcam, ab66043, 1:100), anti-αSMA (Abcam, ab5694, 1:100), anti-Smad2/3 (Cell Signaling, #8685, 1:300), anti-phospho-Smad2/3 (Cell Signaling, #8828, 1:200), anti-BRD4 (Millipore, ABE1391, 1:100), and anti-CDK9 (Santa Cruz, sc-484, 1:100). Fluorescent secondary antibodies utilized were highly cross-adsorbed goat anti-rabbit IgG or goat anti-mouse IgG conjugated to AlexaFluor (AF)- 568 or AF-488 (Molecular Probes). Cell Signaling antibodies (Anti-Smad2/3 and anti -phospho-Smad2/3) and Santa Cruz antibody (anti-CDK9) were also used for Western blots. Other antibodies used in Western

blot analyses were raised against BRD4 (Invitrogen, 23476, 1:1000), GAPDH (Millipore, MAB374, 1:1000) and β-actin (Sigma, A5316, 1:5000) or were HRP-conjugated secondary antibodies (GE Healthcare) raised against rabbit or mouse IgGs. For XChIP analysis, anti-P-Smad3 (Cell Signaling, #9520), anti- BRD4 (Millipore), anti- CDK9 (Santa Cruz) and anti- Phospho-Pol II (Abcam, ab5095) antibodies were used.

Quantitative RT-PCR

hDF and NBS/HTS fibroblasts were seeded in 6-well plates at 80% confluency and serum starved overnight with media containing 1% FBS. For experiments involving inhibitors, LY2157299 (10 μM), GKT137831 (20 μM) and JQ1 (0.5-1 μM) were added to media 1 h before TGFβ while Can508 (30 μM) was added 6 h before to ensure maximum inhibition. Fibroblasts were stimulated with hTGFβ1 for 24-48 h. Cellular RNA was extracted from fibroblasts using Tri Reagent (Sigma) according to manufacturer's instructions and 1 μg RNA was reverse transcribed using Super Script III First-Strand Synthesis System (Invitrogen). The resultant cDNA was diluted 1:2 with RNAase free water and 1 μl cDNA was amplified in a 10 μl reaction containing 5 μl SYBR Green Super Mix and 500 nM primers. The reaction mixtures were aliquoted in triplicates into a Bio-Rad 96-well plate. Bio-Rad CFX96 Real-Time thermal cycler was used to run the real-time reactions according to the following protocol: 95° C for 3 minutes, followed by 40 cycles of 10 s at 95° C, 30 s at 55° C, and the reaction was terminated at 95° C for 10 s. PCR products were subjected to melting curve analysis to ensure that only a single product was formed. Changes in gene expression were determined using ΔΔCT method. DNA Polymerase β was utilized as the housekeeping gene. The human primers used in the qPCR reactions were, SM22 forward: CCGTGGAGATCCCAACTGG, SM22 reverse: CCATCTGAAGGCCAATGACAT; Nox4 forward: CAGATGTTGGGGCTAGGATTG, Nox4 reverse: GAGTGTTCGGCACATGGGTA; fibronectin forward: AGGAAGCCGAGGTTTTAACTG, fibronectin reverse:

AGGACGCTCATAAGTGTCACC; Col1α1 forward: GTGCGATGACGTGATCTGTGA, Col1α1 reverse: CGGTGGTTTCTTGGTCGGT; Smad3 forward: CCATCTCCTACTACGAGCTGAA, Smad3 reverse: CACTGCTGCATTCCTGTTGAC; BRD4 forward: ACCTCCAACCCTAACAAGCC, BRD4 reverse: TTTCCATAGTGTCTTGAGCACC; CDK9 forward: GGGCTGTTGAGCAATGTTTTG, CDK9 reverse: GCAGGATCTTGTTTCTGTGGA; DNA polymerase β forward: CCGCAGGAGACTCTCAACG, DNA polymerase β reverse: GTACTTGTGGATAGCTTGGCTC.

Western blot

Fibroblast cells were scraped into Eppendorf tubes and lysed in RIPA buffer (150 mM NaCl, 1% Triton X-100, 0.5% sodium deoxycholate, 0.1% SDS, 50 mM Tris, pH 8) containing protease (Sigma, P8340) and phosphatase inhibitor cocktails (Thermoscientific, #1861277). Cellular extracts were sonicated for 10s to ensure complete cell lysis and kept on ice for 30 min. DNA was pelleted by centrifugation at 12 000g at 4°C for 20 min and supernatant was transferred to a separate tube. Protein samples were kept frozen at -80°C until needed for analysis.

Protein concentrations were measured using Bradford Protein assay (Protein Reagent, Bio-Rad). 30-50 μg protein was fractionated by 10% SDS-PAGE and transferred to PVDF membrane. After blocking with 5% milk in TBS-Tween (TBS-T) for 1 h, membranes were incubated with primary antibody overnight at 4°C. Membranes were washed thoroughly the next day in TBS-T and incubated with HRP-conjugated secondary antibody for 1 h. ECL Western blot solution (Amersham) was used as the chemiluimesence substrate and the exposed X-ray film was developed with a Kodak machine.

Immunohistochemistry on tissue sections

Tissue sections of skin biopsies from HTS and NBS regions were deparraffinized and rehydrated and antigen retrieval was performed with 10 mM Sodium Citrate, pH 6. Sections were blocked with 5% goat serum in TBS-T for 1h and incubated with primary antibody overnight at 4C. After washing 3x with TBS-T, sections were incubated with a fluorescent secondary antibody (AF-568 goat anti- rabbit) for detection of αSMA or a biotinylated secondary antibody for detecting TGFβ for 1 h. For detection via immunofluorescence, tissue sections were washed again with TBS-T, incubated with DAPI (Molecular Probes) for nuclear counterstaining and glass coverslips were mounted using Dako Fluorescence Mounting Medium. For chromogen based detection, tissue sections were incubated with avidin-biotin complex (Vector Labs, PK6101) followed by exposure to DAB substrate (Vector Labs, SK4100) and counterstaining with hematoxylin. Sections were dehydrated with serial washes in ethanol and xylene before mounting of coverslips. Immunostained sections were evaluated using a Nikon Eclipse 80i microscope and images were captured with an attached Nikon DSM1200F digital camera. ImageJ (NIH) software was used to make composite images and to add the scale bar.

Immunocytochemistry

Fibroblast cells were seeded on coverslips at 30-40% confluency, serum starved for 16 h and stimulated with TGFβ (10 ng/ml) in the presence or absence of an inhibitor. Similar to the qRT-PCR experiments, cells were pre-incubated with LY2157299 (10 μM), GKT137831 (20 μM), JQ1 (0.5-1 μM) or Can508 (30 μM) before TGFβ stimulation. After 24-48 h incubation, cells were fixed in 4% paraformaldehyde and permeablized with 0.25% Triton X-100. Cells were then blocked with 5% goat serum for 1 h, incubated with primary antibody overnight at 4°C, followed by 1 h incubation with AF-568 or AF-488 conjugated secondary antibody. For detection of filamentous actin, AF-568 conjugated phalloidin (Molecular Probes) was added to cells after secondary antibody treatment. Cells were

counterstained with DAPI and mounted on to glass slides for analysis. ImageJ (NIH) software was used to make composite images and to add the scale bar.

ROS detection assay

Nox4 activity and ROS was assessed using a DCF-DA assay as described previously with some modifications (58). Briefly, control siRNA or Nox4 siRNA treated cells were seeded at a density of 35K cells/well in a 24-well plate and serum starved before being treated with TGFβ. Cells were washed 2x with PBS and incubated with 10 μM DCF-DA (Molecular Probes, C6827) for 30 min in phenol-red free media. Following incubation with the dye, cell were washed again 2x with PBS and incubated for another hour with fresh media. Plates were read using a Tekan Infinite F200 Pro fluorescence plate reader (ex: 480 nm, em: 520 nm). Each treatment was assessed in quadruplicates and background reading was subtracted to attain the cellular DCF fluorescence value. hDF cells treated with hydrogen peroxide (4.8 nM) for 1 h were used as positive control.

Collagen gel contraction assay

Collagen gel contraction assay was performed as previously reported (59). Briefly, fibroblasts were harvested from 10-cm plates and re-suspended in DMEM containing 1% FBS. 50k fibroblasts were then seeded into collagen matrices along with GKT137831 (20mM), JQ1 (1 mM) or Can508 (30 mM) and cast into wells of a 24-well plate. The collagen gels were released from the edges and left floating in DMEM + 1% FBS ± inhibitors. Experimental groups were assessed in triplicates. Gels were photographed at 0h, 24h and 48h. Calculations based on the 48h time point are reported in this manuscript. ImageJ software (NIH) was used to calculate the change in surface area which is reported as percent of gel contraction.

Co-Immunoprecipitation

Fibroblasts cells were treated with TGFβ (10 ng/ml) for 24h before being lysed with RIPA buffer containing protease inhibitor cocktail (Sigma). Equal amount of proteins were incubated with 4 μg of control IgG or an antigen specific antibody overnight at 4°C under constant agitation. Next day, pre-washed protein-A conjugated magnetic beads (Invitrogen) were added to each sample and samples were incubated for 2 h at 4°C on a tube rotator. Magnetic beads were washed 3x with RIPA buffer and once with PBS. Immune complexes attached to the magnetic beads were pelleted and kept frozen at -80°C until needed for analysis via SID-SRM-MS.

Stable isotope dilution (SID)-selected Reaction Monitoring (SRM)-mass spectrometry (MS)

SID-SRM-MS assays of SMAD3, CDK9, and BRD4 were developed using a workflow described in previous publications. The signature peptides and SRM parameters are listed in Table I. The peptides were chemically synthesized incorporating isotopically labeled [13C615N4] Arginine or [13C615N2] Lysine to a 99% isotopic enrichment (Thermo Scientific). The proteins immunoprecipitated with anti-SMAD3 and anti-BRD4 antibody were captured by protein A magnetic beads (Dynal Inc.). The proteins on the beads were digested with trypsin as described previously (60-62). Briefly, beads were washed with PBS 3x and then resuspended in 100 μL of 50 mM ammonium hydrogen carbonate (pH 7.8) and 40 μL of 0.1 μg/ μL of trypsin was added. The samples were mixed and trypsinized by gentle vortexing overnight at 37° C. After digestion, the supernatant was collected. The beads were washed with 50 μL of 50% acetonitrile (ACN) three times and the supernatant was pooled, and dried. The tryptic digests were then reconstituted in 50 μL of 4% ACN-0.01% TFA. An aliquot of 5 μL of diluted stable isotope labeled signature peptides was added to each tryptic digest. These samples were desalted with ZipTip C18. The peptides were eluted with 80% ACN and dried with Speedvac. The peptides were reconstituted in 30 μL of 5% formic acid-0.01% TFA and were directly used

for LC-SRM-MS analysis without further purification or fractionation. SRM assays were performed on LC-SRM-MS analysis was performed with a TSQ Vantage triple quadrupole mass spectrometer equipped with nanospray source (Thermo Scientific, San Jose, CA) as described (60-62). The online chromatography were performed using an Eksigent NanoLC-2D HPLC system (AB SCIEX, Dublin, CA). An aliquot of 10 µL of each of the tryptic digests was injected on a C18 reverse-phase nano-HPLC column (PicoFrit™, 75 µm x 10 cm; tip ID 15 µm) at a flow rate of 500 nL/min with a 20-min 98% A, followed by a 15-min linear gradient from 2-30% mobile phase B (0.1 % formic acid-90% acetonitrile) in mobile phase A (0.1 % formic acid). The TSQ Vantage was operated in high-resolution SRM mode with Q1 and Q3 set to 0.2 and 0.7-Da Full Width Half Maximum (FWHM). All acquisition methods used the following parameters: 2100 V ion spray voltage, a 275° C ion transferring tube temperature, a collision-activated dissociation pressure at 1.5 mTorr, and the S-lens voltage used the values in S-lens table generated during MS calibration.

All SRM data were manually inspected to ensure peak detection and accurate integration. The chromatographic retention time and the relative product ion intensities of the analyte peptides were compared to those of the stable isotope labeled standard (SIS) peptides. The variation of the retention time between the analyte peptides and their SIS counterparts should be within 0.05 min, and the difference in the relative product ion intensities of the analyte peptides and SIS peptides were below 20%. The peak areas in the extract ion chromatography of the native and SIS version of each signature peptide were integrated using Xcalibur® 2.1. The default values for noise percentage and base-line subtraction window were used. The ratio between the peak area of native and SIS version of each peptide was calculated.

siRNA knockdown of mediators of myofibroblast transdifferentiation

hDF or HTS fibroblast were grown to 90% confluency before being harvested with 0.25% Trypsin. After trypsin neutralization, $1x10^6$ cells were electroporated with 100 pmol of non-specific control siRNA (ON-TARGET plus SMARTpool by Dharmacon) or gene specific siRNA (ON-TARGET plus SMARTpool by Dharmacon targeting Nox4, Smad3, BRD4 or CDK9) using U-023 program (Amaxa). Cells were seeded in 6-well plates or on cover-slips. After 48 hours, cells were serum starved overnight and then treated with TGFβ (10 ng/ml) for 24-48h.

Dual cross-link chromatin immunoprecipitation (XChIP)

XChIP was performed as previously described (63). Briefly, fibroblast cells (~1.2 x 10^6 cells per 10-cm plate) were washed 2x with PBS; protein-protein crosslinks were made with 2 mM disuccinimidyl glutarate (Pierce); and protein-DNA crosslinks were formed with formaldehyde. Chromatin was sheared via 5 rounds of sonication at setting 4 with 10 s breaks on ice in-between pulses (Branson Sonifier 150, Branson Ultrasonics, Danbury, CT). Equal amount of sheared chromatin was immunoprecipitated overnight at 4˚C with 4 μg of control IgG or target specific antibody (anti- Smad3, - P-Smad3, -BRD4, -CDK9 or -P-Pol II). Protein A conjugated magnetic beads (Invitrogen) were added to capture antibody-antigen complexes. Immunoprecipitates were washed and then eluted with elution buffer (0.09 M $NaHCO_3$, 1% SDS). Samples were de-crosslinked in 0.2 M NaCl at 65˚C for 2-3 h. DNA was isolated using phenol-chloroform extraction and ethanol precipitation and re-suspended in TE buffer. Real-time genomic PCR was performed on the isolated DNA using primers specific for the Nox4 promoter: Nox4 5' forward- GGACATCCTGAACAGCAGCA, Nox4 5' reverse- CTGCACCAGTCTGCTCCG. Fold change of DNA in each sample was determined by first, normalizing the absolute value to the input DNA reference and then calculating the fold change relative to unstimulated cells.

Statistical analysis

Differences across multiple groups were analyzed by analysis-of-variance (ANOVA), followed by Newman-Keuls or Tukey's pairwise comparison. $P < 0.05$ was considered statistically significant.

References

1. Rinn JL, Bondre C, Gladstone HB, Brown PO, Chang HY. Anatomic demarcation by positional variation in fibroblast gene expression programs. PLoS Genet. 2006;2(7):e119.
2. Peach MJ. Renin-angiotensin system: biochemistry and mechanisms of action. Physiol Rev. 1977;57(2):313-70.
3. Daugherty A, Rateri DL, Lu H, Inagami T, Cassis LA. Hypercholesterolemia stimulates angiotensin peptide synthesis and contributes to atherosclerosis through the AT1A receptor. Circulation. 2004;110(25):3849-57.
4. Cassis LA, Rateri DL, Lu H, Daugherty A. Bone marrow transplantation reveals that recipient AT1a receptors are required to initiate angiotensin II-induced atherosclerosis and aneurysms. Arterioscler Thromb Vasc Biol. 2007;27(2):380-6.
5. Recinos A, LeJeune WS, Sun H, Lee CY, Tieu BC, Lu M, et al. Angiotensin II induces IL-6 expression and the Jak-STAT3 pathway in aortic adventitia of LDL receptor-deficient mice. Atherosclerosis. 2007;194(1):125-33.
6. Daugherty A, Manning MW, Cassis LA. Angiotensin II promotes atherosclerotic lesions and aneurysms in apolipoprotein E-deficient mice. J Clin Invest. 2000;105(11):1605-12.
7. Saraff K, Babamusta F, Cassis LA, Daugherty A. Aortic dissection precedes formation of aneurysms and atherosclerosis in angiotensin II-infused, apolipoprotein E-deficient mice. Arterioscler Thromb Vasc Biol. 2003;23(9):1621-6.
8. Tieu BC, Lee C, Sun H, Lejeune W, Recinos A, Ju X, et al. An adventitial IL-6/MCP1 amplification loop accelerates macrophage-mediated vascular inflammation leading to aortic dissection in mice. J Clin Invest. 2009;119(12):3637-51.
9. Hirohata A, Yamamoto K, Miyoshi T, Hatanaka K, Hirohata S, Yamawaki H, et al. Impact of olmesartan on progression of coronary atherosclerosis a serial volumetric intravascular ultrasound analysis from the OLIVUS (impact of OLmesarten on progression of coronary atherosclerosis: evaluation by intravascular ultrasound) trial. J Am Coll Cardiol. 2010;55(10):976-82.
10. Kristensen KE, Torp-Pedersen C, Gislason GH, Egfjord M, Rasmussen HB, Hansen PR. Angiotensin-converting enzyme inhibitors and angiotensin II receptor blockers in patients with abdominal aortic aneurysms: nation-wide cohort study. Arterioscler Thromb Vasc Biol. 2015;35(3):733-40.
11. Baker RG, Hayden MS, Ghosh S. NF-κB, inflammation, and metabolic disease. Cell Metab. 2011;13(1):11-22.
12. Brasier AR. The nuclear factor-kappaB-interleukin-6 signalling pathway mediating vascular inflammation. Cardiovasc Res. 2010;86(2):211-8.
13. Gilmore TD. Introduction to NF-kappaB: players, pathways, perspectives. Oncogene. 2006;25(51):6680-4.
14. Jamaluddin M, Wang S, Boldogh I, Tian B, Brasier AR. TNF-alpha-induced NF-kappaB/RelA Ser(276) phosphorylation and enhanceosome formation is mediated by an ROS-dependent PKAc pathway. Cell Signal. 2007;19(7):1419-33.

15. Cui R, Tieu B, Recinos A, Tilton RG, Brasier AR. RhoA mediates angiotensin II-induced phospho-Ser536 nuclear factor kappaB/RelA subunit exchange on the interleukin-6 promoter in VSMCs. Circ Res. 2006;99(7):723-30.
16. Zhang L, Cheng J, Ma Y, Thomas W, Zhang J, Du J. Dual pathways for nuclear factor kappaB activation by angiotensin II in vascular smooth muscle: phosphorylation of p65 by IkappaB kinase and ribosomal kinase. Circ Res. 2005;97(10):975-82.
17. Choudhary S, Lu M, Cui R, Brasier AR. Involvement of a novel Rac/RhoA guanosine triphosphatase-nuclear factor-kappaB inducing kinase signaling pathway mediating angiotensin II-induced RelA transactivation. Mol Endocrinol. 2007;21(9):2203-17.
18. Jones KG, Brull DJ, Brown LC, Sian M, Greenhalgh RM, Humphries SE, et al. Interleukin-6 (IL-6) and the prognosis of abdominal aortic aneurysms. Circulation. 2001;103(18):2260-5.
19. Dawson J, Cockerill GW, Choke E, Belli AM, Loftus I, Thompson MM. Aortic aneurysms secrete interleukin-6 into the circulation. J Vasc Surg. 2007;45(2):350-6.
20. Hou T, Tieu BC, Ray S, Recinos Iii A, Cui R, Tilton RG, et al. Roles of IL-6-gp130 Signaling in Vascular Inflammation. Curr Cardiol Rev. 2008;4(3):179-92.
21. Tsou CL, Peters W, Si Y, Slaymaker S, Aslanian AM, Weisberg SP, et al. Critical roles for CCR2 and MCP-3 in monocyte mobilization from bone marrow and recruitment to inflammatory sites. J Clin Invest. 2007;117(4):902-9.
22. Tieu BC, Ju X, Lee C, Sun H, Lejeune W, Recinos A, et al. Aortic adventitial fibroblasts participate in angiotensin-induced vascular wall inflammation and remodeling. J Vasc Res. 2011;48(3):261-72.
23. Zheng B, Zhang Z, Black CM, de Crombrugghe B, Denton CP. Ligand-dependent genetic recombination in fibroblasts : a potentially powerful technique for investigating gene function in fibrosis. Am J Pathol. 2002;160(5):1609-17.
24. Muzumdar MD, Tasic B, Miyamichi K, Li L, Luo L. A global double-fluorescent Cre reporter mouse. Genesis. 2007;45(9):593-605.
25. Singer AJ, Clark RA. Cutaneous wound healing. N Engl J Med. 1999;341(10):738-46.
26. van der Veer WM, Bloemen MC, Ulrich MM, Molema G, van Zuijlen PP, Middelkoop E, et al. Potential cellular and molecular causes of hypertrophic scar formation. Burns. 2009;35(1):15-29.
27. Arno AI, Gauglitz GG, Barret JP, Jeschke MG. Up-to-date approach to manage keloids and hypertrophic scars: a useful guide. Burns. 2014;40(7):1255-66.
28. Davis J, Molkentin JD. Myofibroblasts: trust your heart and let fate decide. J Mol Cell Cardiol. 2014;70:9-18.
29. Ijaz T, Pazdrak K, Kalita M, Konig R, Choudhary S, Tian B, et al. Systems biology approaches to understanding Epithelial Mesenchymal Transition (EMT) in mucosal remodeling and signaling in asthma. World Allergy Organ J. 2014;7(1):13.
30. Takac I, Schröder K, Zhang L, Lardy B, Anilkumar N, Lambeth JD, et al. The E-loop is involved in hydrogen peroxide formation by the NADPH oxidase Nox4. J Biol Chem. 2011;286(15):13304-13.
31. Hecker L, Vittal R, Jones T, Jagirdar R, Luckhardt TR, Horowitz JC, et al. NADPH oxidase-4 mediates myofibroblast activation and fibrogenic responses to lung injury. Nat Med. 2009;15(9):1077-81.

32. Bai G, Hock TD, Logsdon N, Zhou Y, Thannickal VJ. A far-upstream AP-1/Smad binding box regulates human NOX4 promoter activation by transforming growth factor-β. Gene. 2014;540(1):62-7.
33. Jiang JX, Chen X, Serizawa N, Szyndralewiez C, Page P, Schröder K, et al. Liver fibrosis and hepatocyte apoptosis are attenuated by GKT137831, a novel NOX4/NOX1 inhibitor in vivo. Free Radic Biol Med. 2012;53(2):289-96.
34. Zhao QD, Viswanadhapalli S, Williams P, Shi Q, Tan C, Yi X, et al. NADPH oxidase 4 induces cardiac fibrosis and hypertrophy through activating Akt/mTOR and NFκB signaling pathways. Circulation. 2015;131(7):643-55.
35. Jonkers I, Lis JT. Getting up to speed with transcription elongation by RNA polymerase II. Nat Rev Mol Cell Biol. 2015;16(3):167-77.
36. Shi J, Vakoc CR. The mechanisms behind the therapeutic activity of BET bromodomain inhibition. Mol Cell. 2014;54(5):728-36.
37. Devaiah BN, Lewis BA, Cherman N, Hewitt MC, Albrecht BK, Robey PG, et al. BRD4 is an atypical kinase that phosphorylates serine2 of the RNA polymerase II carboxy-terminal domain. Proc Natl Acad Sci U S A. 2012;109(18):6927-32.
38. Lewandoski M, Wassarman KM, Martin GR. Zp3-cre, a transgenic mouse line for the activation or inactivation of loxP-flanked target genes specifically in the female germ line. Curr Biol. 1997;7(2):148-51.
39. Beg AA, Sha WC, Bronson RT, Ghosh S, Baltimore D. Embryonic lethality and liver degeneration in mice lacking the RelA component of NF-kappa B. Nature. 1995;376(6536):167-70.
40. Moore-Morris T, Guimarães-Camboa N, Banerjee I, Zambon AC, Kisseleva T, Velayoudon A, et al. Resident fibroblast lineages mediate pressure overload-induced cardiac fibrosis. J Clin Invest. 2014;124(7):2921-34.
41. Ijaz T, Sun H, Pinchuk IV, Milewicz DM, Tilton RG, Brasier AR. Deletion of NF-κB/RelA in Angiotensin II-Sensitive Mesenchymal Cells Blocks Aortic Vascular Inflammation and Abdominal Aortic Aneurysm Formation. Arterioscler Thromb Vasc Biol. 2017.
42. Manea A, Tanase LI, Raicu M, Simionescu M. Transcriptional regulation of NADPH oxidase isoforms, Nox1 and Nox4, by nuclear factor-kappaB in human aortic smooth muscle cells. Biochem Biophys Res Commun. 2010;396(4):901-7.
43. Tian B, Zhao Y, Sun H, Zhang Y, Yang J, Brasier AR. BRD4 mediates NF-κB-dependent epithelial-mesenchymal transition and pulmonary fibrosis via transcriptional elongation. Am J Physiol Lung Cell Mol Physiol. 2016;311(6):L1183-L201.
44. Ding N, Hah N, Yu RT, Sherman MH, Benner C, Leblanc M, et al. BRD4 is a novel therapeutic target for liver fibrosis. Proc Natl Acad Sci U S A. 2015;112(51):15713-8.
45. Nowak DE, Tian B, Jamaluddin M, Boldogh I, Vergara LA, Choudhary S, et al. RelA Ser276 phosphorylation is required for activation of a subset of NF-kappaB-dependent genes by recruiting cyclin-dependent kinase 9/cyclin T1 complexes. Mol Cell Biol. 2008;28(11):3623-38.
46. Tang X, Peng R, Phillips JE, Deguzman J, Ren Y, Apparsundaram S, et al. Assessment of Brd4 inhibition in idiopathic pulmonary fibrosis lung fibroblasts and in vivo models of lung fibrosis. Am J Pathol. 2013;183(2):470-9.

47. Ray S, Ju X, Sun H, Finnerty CC, Herndon DN, Brasier AR. The IL-6 trans-signaling-STAT3 pathway mediates ECM and cellular proliferation in fibroblasts from hypertrophic scar. J Invest Dermatol. 2013;133(5):1212-20.
48. Cucoranu I, Clempus R, Dikalova A, Phelan PJ, Ariyan S, Dikalov S, et al. NAD(P)H oxidase 4 mediates transforming growth factor-beta1-induced differentiation of cardiac fibroblasts into myofibroblasts. Circ Res. 2005;97(9):900-7.
49. Piera-Velazquez S, Makul A, Jiménez SA. Increased expression of NAPDH oxidase 4 in systemic sclerosis dermal fibroblasts: regulation by transforming growth factor β. Arthritis Rheumatol. 2015;67(10):2749-58.
50. Lévigne D, Modarressi A, Krause KH, Pittet-Cuénod B. NADPH oxidase 4 deficiency leads to impaired wound repair and reduced dityrosine-crosslinking, but does not affect myofibroblast formation. Free Radic Biol Med. 2016;96:374-84.
51. Rozycki M, Bialik JF, Speight P, Dan Q, Knudsen TE, Szeto SG, et al. Myocardin-related Transcription Factor Regulates Nox4 Protein Expression: LINKING CYTOSKELETAL ORGANIZATION TO REDOX STATE. J Biol Chem. 2016;291(1):227-43.
52. Katsuyama M, Hirai H, Iwata K, Ibi M, Matsuno K, Matsumoto M, et al. Sp3 transcription factor is crucial for transcriptional activation of the human NOX4 gene. FEBS J. 2011;278(6):964-72.
53. Tian B, Zhao Y, Kalita M, Edeh CB, Paessler S, Casola A, et al. CDK9-dependent transcriptional elongation in the innate interferon-stimulated gene response to respiratory syncytial virus infection in airway epithelial cells. J Virol. 2013;87(12):7075-92.
54. Ijaz T, Jamaluddin M, Zhao Y, Zhang Y, Jay J, Finnerty CC, et al. Coordinate activities of BRD4 and CDK9 in the transcriptional elongation complex are required for TGFβ-induced Nox4 expression and myofibroblast transdifferentiation. Cell Death Dis. 2017;8(2):e2606.
55. Ijaz T, Wakamiya M, Sun H, Recinos A, Tilton RG, Brasier AR. Generation and characterization of a novel transgenic mouse harboring conditional nuclear factor-kappa B/RelA knockout alleles. BMC Dev Biol. 2016;16(1):32.
56. Ju X, Ijaz T, Sun H, Ray S, Lejeune W, Lee C, et al. Interleukin-6-signal transducer and activator of transcription-3 signaling mediates aortic dissections induced by angiotensin II via the T-helper lymphocyte 17-interleukin 17 axis in C57BL/6 mice. Arterioscler Thromb Vasc Biol. 2013;33(7):1612-21.
57. Zhang Z, Finnerty CC, He J, Herndon DN. Smad ubiquitination regulatory factor 2 expression is enhanced in hypertrophic scar fibroblasts from burned children. Burns. 2012;38(2):236-46.
58. Cai H, Dikalov S, Griendling KK, Harrison DG. Detection of reactive oxygen species and nitric oxide in vascular cells and tissues: comparison of sensitivity and specificity. Methods Mol Med. 2007;139:293-311.
59. Ngo P, Ramalingam P, Phillips JA, Furuta GT. Collagen gel contraction assay. Methods Mol Biol. 2006;341:103-9.
60. Zhao Y, Brasier AR. Applications Of Selected Reaction Monitoring (SRM)-Mass Spectrometry (MS) For Quantitative Measurement Of Signaling Pathways. Methods. 2013.
61. Zhao Y, Tian B, Edeh CB, Brasier AR. Quantitation of the dynamic profiles of the innate immune response using multiplex selected reaction monitoring-mass spectrometry. Molecular & cellular proteomics : MCP. 2013;12:1513-29.

62. Zhao YX, Widen SG, Jamaluddin M, Tian B, Wood TG, Edeh CB, et al. Quantification of Activated NF-kappa B/RelA Complexes Using ssDNA Aptamer Affinity - Stable Isotope Dilution-Selected Reaction Monitoring-Mass Spectrometry. Molecular & Cellular Proteomics. 2011;10(6).
63. Tian B, Yang J, Brasier AR. Two-step cross-linking for analysis of protein-chromatin interactions. Methods Mol Biol. 2012;809:105-20.